catalysts

MDPI

Article

Electronic Tuning of Sterically Encumbered 2-(Arylimino)Pyridine-Nickel Ethylene Polymerization Catalysts by *Para*-Group Modification

Zahra Hosseinzadeh [1], Ming Liu [1], Qiuyue Zhang [1], Tongling Liang [1], Gregory A. Solan [2,*], Yanping Ma [1] and Wen-Hua Sun [1,*]

[1] Key Laboratory of Engineering Plastics and Beijing National Laboratory for Molecular Sciences, Institute of Chemistry Chinese Academy of Sciences, Beijing 100190, China
[2] Department of Chemistry, University of Leicester, University Road, Leicester LE1 7RH, UK
* Correspondence: gas8@leicester.ac.uk (G.A.S.); whsun@iccas.ac.cn (W.-H.S.); Tel.: +44-(0)-116-252209 (G.A.S); Tel.: +86-10-6255-7955 (W.-H.S.)

Abstract: A collection of five related 2-(arylimino)pyridines, 2-{(2,6-(CH(C_6H_4-*p*-F)$_2$)$_2$-4- RC_6H_2)N=CMe}C_5H_4N, each *ortho*-substituted with 4,4′-difluorobenzhydryl groups but distinct in the electronic properties of the *para*-R substituent (R = Me **L1**, Et **L2**, *i*-Pr **L3**, F **L4**, OCF_3 **L5**), were prepared and combined with (DME)$NiBr_2$ to form their corresponding $LNiBr_2$ complexes, **Ni1**–**Ni5**, in high yields. All the complexes were characterized by FT-IR, ^{19}F NMR spectroscopy and elemental analysis, while **Ni5** was additionally the subject of an X-ray determination, revealing a bromide-bridged dimer. The molecular structure of *bis*-ligated (**L4**)$_2NiBr_2$ (**Ni4′**) was also determined, the result of ligand reorganization having occurred during attempted crystallization of **Ni4**. On activation with either $EtAlCl_2$ or MMAO, **Ni1**–**Ni5** exhibited high catalytic activities (up to 4.28 × 10^6 g of PE (mol of Ni)$^{-1}$ h^{-1} using $EtAlCl_2$) and produced highly branched polyethylene exhibiting low molecular weight (M_w range: 2.50–6.18 kg·mol^{-1}) and narrow dispersity (M_w/M_n range: 2.21–2.90). Notably, it was found that the type of *para*-R group impacted on catalytic performance with **Ni5** > **Ni4** > **Ni3** > **Ni1** > **Ni2** for both co-catalysts, underlining the positive influence of electron withdrawing substituents. Analysis of the structural composition of the polyethylene by ^{1}H and ^{13}C NMR spectroscopy revealed the existence of vinyl-end groups (–CH=CH_2) and high levels of internal unsaturation (–CH=CH–) (ratio of vinylene to vinyl, range: 3.1:1–10.3:1) along with various types of branch (Me, Et, Pr, Bu, 1,4-paired Me, 1,6-paired Me and LCBs). Furthermore, reaction temperature was shown to greatly affect the end group type, branching density, molecular weight and in turn the melting points of the resulting polyethylenes.

Keywords: nickel; 2-(arylimino)pyridines; steric bulk; electronic effects; ethylene; branched polyethylene

check for updates

Citation: Hosseinzadeh, Z.; Liu, M.; Zhang, Q.; Liang, T.; Solan, G.A.; Ma, Y.; Sun, W.-H. Electronic Tuning of Sterically Encumbered 2-(Arylimino)Pyridine-Nickel Ethylene Polymerization Catalysts by *Para*-Group Modification. *Catalysts* **2022**, *12*, 1520. https://doi.org/10.3390/catal12121520

Academic Editor: Marc Visseaux

Received: 31 October 2022
Accepted: 23 November 2022
Published: 25 November 2022

1. Introduction

The application of group 10 metal (Ni, Pd) catalyzed ethylene polymerization has been thoroughly studied for more than 25 years [1–3], following the pioneering disclosure that their α-diimine complexes can promote the formation of high molecular weight polyethylene (PE) [3–9]. Moreover, their low oxophilicity when compared to early transition metal complexes and their unique ability to mediate a "chain-walking" pathway to form branched PE makes this class of polymerization catalyst particularly attractive [4,10–14]. Furthermore, through a choice of the *N*,*N*-ligand, reaction parameters and group 10 metal center, there offers a means to precisely control the polymer architecture (linear, hyperbranched or dendritic PEs) and in turn access some practically important polymeric materials [4,15–18].

With particular regard to the α-diimine ligand structure, structural modifications in the form of steric and electronic variations to the ligand backbone and/or the *N*-aryl substituents can have a significant impact on the activity of the metal catalyst and resulting

polymer properties [19–21]. One early example relates to nickel precatalysts bearing 2-(arylimino)pyridines (**A**, Figure 1), where the steric hindrance imparted by the *ortho*-substituents of the *N*-aryl rings (e.g., Me, *i*-Pr) can engender good activity on the ethylene polymerization catalyst [22]. In related work, the presence of electron-withdrawing groups at the *para*-position of the *N*-aryl ring have been shown to increase the catalytic performance, whilst also affecting molecular weight and dispersity of the polymer [23,24]. Recent developments involving 2-iminopyridyl-nickel catalysts have seen the incorporation of even more sterically hindered benzhydryl ($CHPh_2$) substituents to the 2,7-positions on an *N*-naphthyl ring (**B**, Figure 1). By comparison, the introduction of dibenzocyclopentyl substituents to the *para* position of the *N*-aryl group displayed poorer performance and lower molecular weight (**C**, Figure 1). Alternatively, by fusion of a cyclooctyl group to the iminopyridine backbone (**D**, Figure 1), the activity of the resulting nickel catalyst decreased while the molecular weight of the polymer increased. More recent developments involving 2-iminopyridyl-nickel catalysts have seen the addition of sterically hindered dibenzosuberyl substituents to the 2,4-positions of the *N*-aryl group in **E** (Figure 1) [24] resulting in high catalytic activity and high molecular weight polymer [25–28]. Furthermore, our group has recently studied the impact of electronic variations made to the *ortho*-R group in **E** (Figure 1) and have demonstrated the positive effects of introducing electron-withdrawing substituents (e.g., R = Cl, F) [23]. Elsewhere, the benefits of *para*-substituted trifluoromethoxy (OCF_3) groups have seen the disclosure of both highly active nickel catalysts [25,29], along with improved thermal stability.

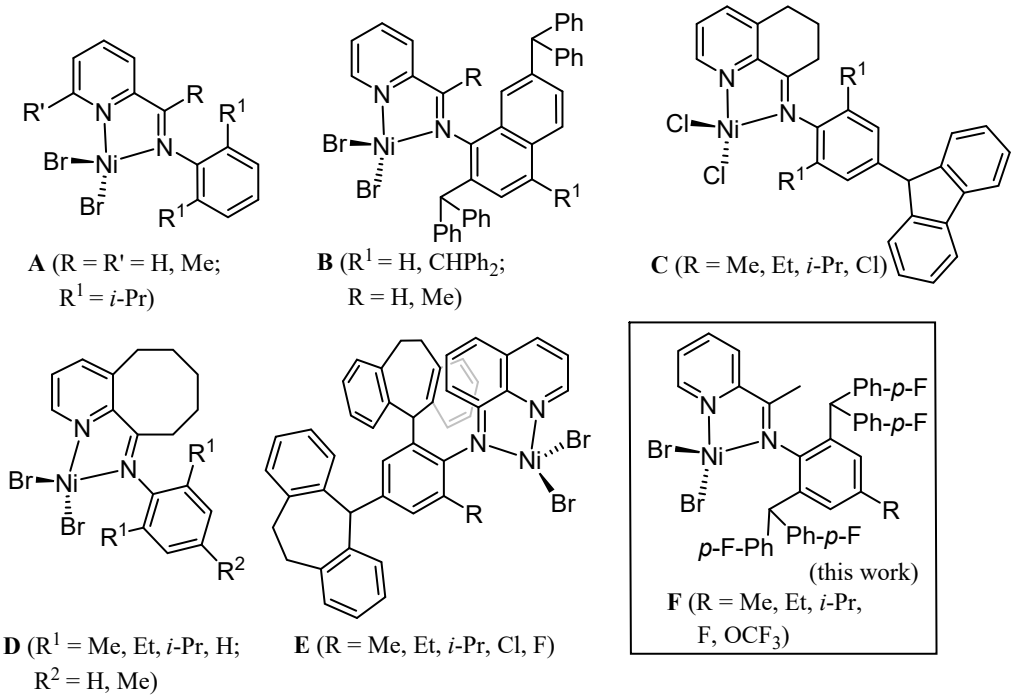

Figure 1. 2-(Arylimino)pyridine-nickel(II) halide (**A**), its substituted derivatives, (**B**–**E**), and the target of this work, (**F**).

On account of the positive effects of introducing fluorine and fluorine-containing substituents to the *N*,*N*-ligand manifold [26], herein we report a new family of 2-(arylimino)pyridine-nickel precatalysts containing *ortho*-benzhydryl groups decorated with fluorine atoms at the *para*-positions of their aryl rings (**F**, Figure 1). Specifically, five examples of **F** are disclosed in which the *para*-R group of the *N*-aryl group is systematically varied to include methyl, ethyl, isopropyl, fluoro and trifluoromethoxy. An in-depth polymerization study is then performed with the aim to explore any correlations between the *para*-R substituent and catalytic activity and polymer properties. Furthermore, to understand how the structural variations reported in this study compare with previous reports, the data generated for **F**

are compared with **C**, **D** and **E**. In addition, full synthetic details for the new ligands and complexes developed in the work are described.

2. Results and Discussion

2.1. Synthesis and Characterization of L1–L5 and Their Complexes Ni1–Ni5

Five novel examples of 4,4′-difluorobenzhydryl-substituted 2-(arylimino)pyridines, 2-{(2,6-(CH(C_6H_4-*p*-F)$_2$)$_2$-4-RC_6H_2)N=CMe}C_5H_4N (R = Me **L1**, Et **L2**, *i*-Pr **L3**, F **L4**, and OCF_3 **L5**), were synthesized by a two-step procedure involving firstly the reaction of 2-acetylpyridine with 2,6-(CH(C_6H_4-*p*-F)$_2$)$_2$-4-R$C_6H_2NH_2$ (R = Me **A1**, Et **A2**, *i*-Pr **A3**, F **A4**, OCF_3 **A5**) in the presence of zinc(II) chloride, and secondly demetallation of the resulting zinc intermediate with aqueous potassium carbonate (Scheme 1). Following work-up, **L1**–**L5** could be isolated in reasonable yields (55–74%) and characterized by FT-IR, ^{1}H, ^{19}F and ^{13}C NMR spectroscopies and elemental analysis.

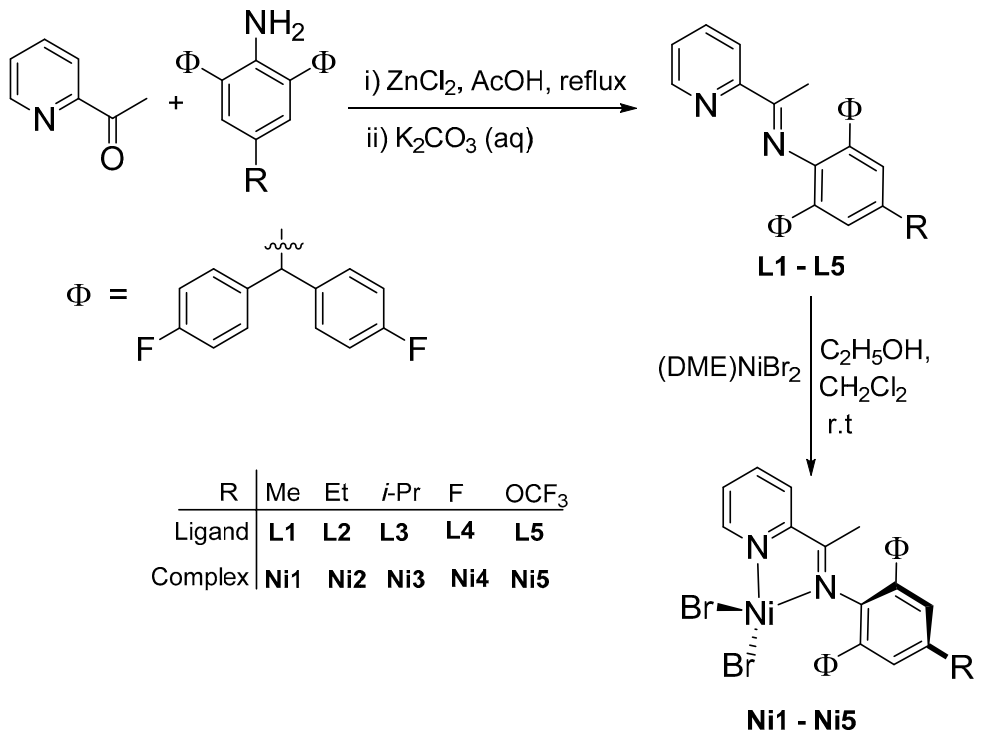

Scheme 1. Synthetic route to 2-(arylimino)pyridines, **L1**–**L5** and their corresponding nickel(II) bromide complexes, **Ni1**–**Ni5**.

Next, the interaction of **L1**–**L5** with (DME)$NiBr_2$ (DME = 1,2-dimethoxyethane) in a mixture of ethanol and dichloromethane at room temperature gave [2-{(2,6-(CH(C_6H_4-*p*-F)$_2$)$_2$-4-RC_6H_2)N=CMe}C_5H_4N]$NiBr_2$ (R = Me **Ni1**, Et **Ni2**, *i*-Pr **Ni3**, F **Ni4**, OCF_3 **Ni5**) in good yield (82–91%) (Scheme 1). All complexes proved air-stable and were amenable to characterization by FT-IR, ^{19}F NMR spectroscopy and elemental analysis. In addition, **Ni5** and a derivative of **Ni4** have been the subject of single crystal X-ray diffraction studies.

Single crystals of **Ni5** suitable for X-ray determination were grown by slow diffusion of diethyl ether into a dichloromethane solution containing the complex at room temperature. Unexpectedly, a similar slow diffusion approach using **Ni4** resulted in the formation of a few crystals of (**L4**)$_2$$NiBr_2$ (**Ni4′**); it is presumed that ligand reorganization occurred during the crystallization process. Both structures are distinct (Figures 2 and 3) and will be discussed separately; selected bond distances and angles for each are given in Table 1.

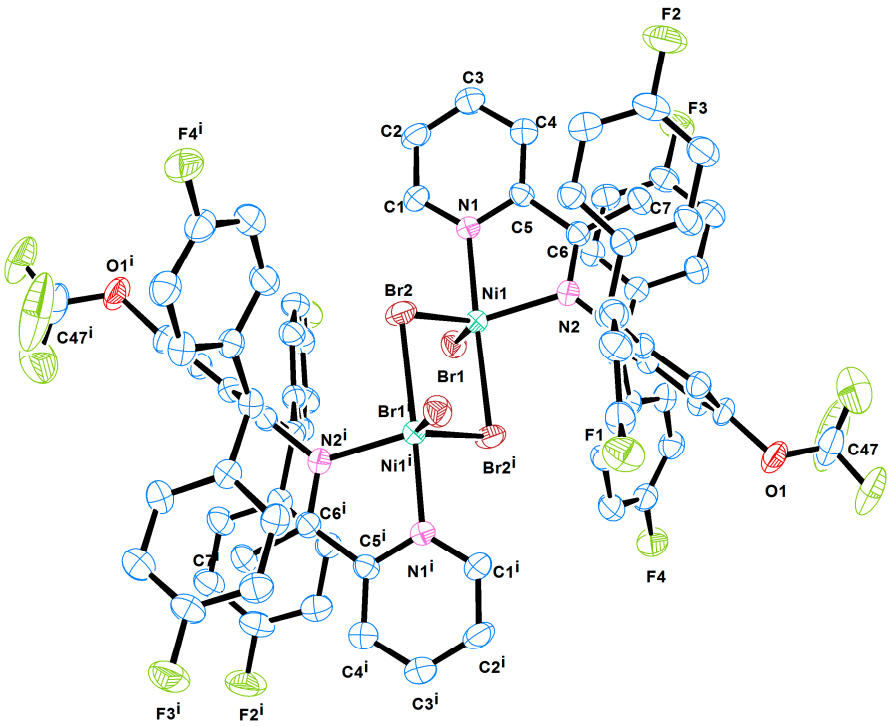

Figure 2. ORTEP drawing of **Ni5** with thermal ellipsoids shown at a probability level of 30%. All the hydrogen atoms have been omitted for clarity. The atoms labelled with an 'i' superscript have been generated by symmetry.

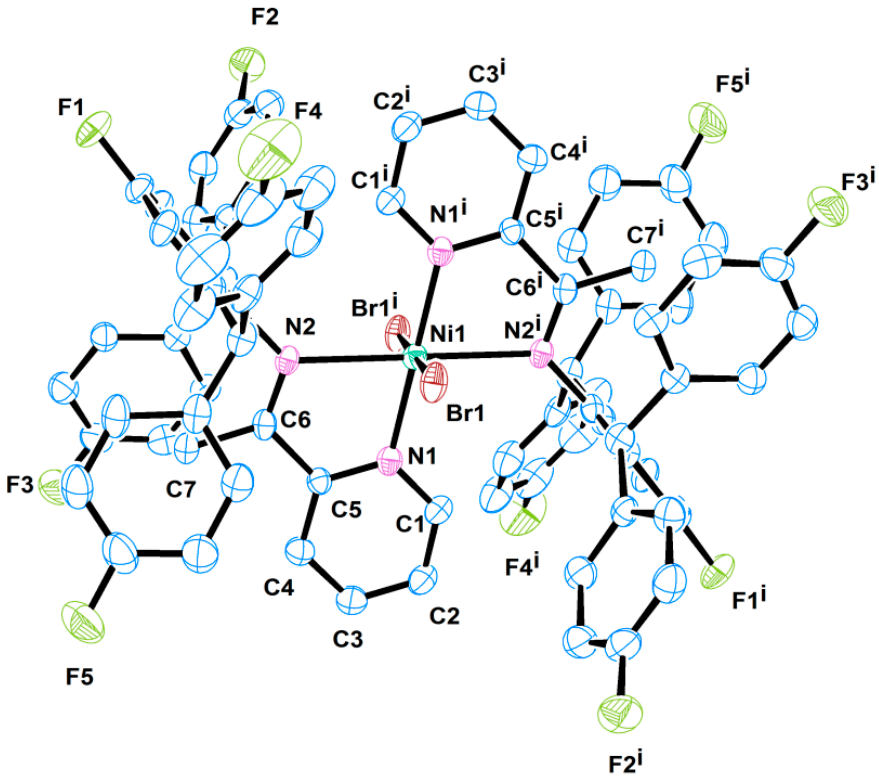

Figure 3. ORTEP drawing of bis-ligated **Ni4′** with thermal ellipsoids shown at a probability level of 30%. All the hydrogen atoms have been omitted for clarity. The atoms labelled with an 'i' superscript have been generated by symmetry.

Table 1. Selected bond lengths (Å) and angles (°) for **Ni5** and **Ni4′**.

Ni5		**Ni4′**	
Bond lengths (Å)			
Ni1-Br1	2.5196 (8)	Ni1-Br1	2.5176 (5)
Ni1-Br2	2.3857 (8)	Ni1-N1	2.020 (4)
Ni1-N1	2.042 (3)	Ni1-N2	2.365 (3)
Ni1-N2	2.055 (3)	N2-C6	1.286 (6)
N2-C6	1.298 (5)	N2-C8	1.449 (5)
N2-C8	1.438 (5)		
O1-C47	1.312(5)		
Bond angles (°)			
N1-Ni1-N2	79.24 (13)	N1-Ni1-N2	75.86 (14)
Br2-Ni1-Br1	128.92 (3)	N1-Ni1-Br1	90.96 (10)
Br2-Ni1-Br1^{i}	95.80 (3)	N2-Ni1-Br1	91.92 (9)
Br1-Ni1-Br1^{i}	84.55 (3)	N1^{i}-Ni1-Br1	89.04 (10)
N2-Ni1-Br2	110.91 (10)	N2^{i}-Ni1-Br1	88.08 (9)
N2-Ni1-Br1	119.64 (10)	N1-Ni1-N2^{i}	104.14 (14)
N2-Ni1-Br1^{i}	97.98 (10)	N1-Ni1-N1^{i}	180.00 (19)
N1-Ni1-Br2	91.29 (10)	N2^{i}-Ni1-N2	180.00 (16)

The atoms labelled with an 'i' superscript have been generated by symmetry.

The structure of **Ni5** has been generated by symmetry and comprises an Ni(μ-Br)$_2$Ni core, with each nickel center additionally coordinated by a bromide ligand and an *N*,*N*-bound **L5**; the two metals are positioned at a distance of 3.749 Å apart (Figure 2). The geometry about each nickel center can be best described as trigonal bipyramidal, with Br1, Br2 and N2 defining the equatorial belt and Br2^{i} and N1 defining the axial sites. The Ni-Br distances show some variation (Ni1-Br1 2.5196(8) vs. Ni1-Br2 2.3857(8) Å) on account of their distinct bonding modes (bridging vs. terminal), while their Ni-N distances are comparable (Ni1-N$_{pyridine}$ 2.042(3) vs. Ni1-Ni2$_{imine}$ 2.055(3) Å). The five-membered chelate ring formed by Ni1, N1, N2, C5 and C6 is almost co-planar (max. deviation from plane = 0.019 Å), while the planes of the pyridine and *N*-aryl group are near perpendicular (dihedral angle = 87.72°). Related dimeric structures of the type (N,N)NiX(μ-X)$_2$NiX(N,N) are fairly common in the literature for this class of complex [16]. In terms of the *para*-OCF$_3$ group, this adopts a skew conformation with respect the adjacent arene ring (C–C–O–C dihedral angle 66.8°), while the distance between the CF$_3$ carbon and the neighboring oxygen atom in [1.312(5) Å] suggests some double bond character [30]. There are no intermolecular contacts of note.

For **Ni4′**, the structure was also generated by symmetry and consisted of a single nickel center surrounded by two *N*,*N*-chelating **L4** ligands and two *trans*-disposed bromide ligands to form a distorted octahedral geometry; related *bis*-chelated structural types have been previously reported [29,31,32]. Dissimilar to that in **Ni5**, the Ni-N bond lengths show some variation with Ni-N$_{pyridine}$ (2.020(4) Å), noticeably shorter than the Ni-N$_{imine}$ (2.365(3) Å), an observation that is presumably attributable to the higher coordination number in **Ni4′** and the steric properties exerted by the *ortho*-4,4′-difluorobenzydryl groups. Nonetheless, the five-membered chelate ring formed by Ni1, N1, C5, N2 and C6 is essentially co-planar, with C5 and C6 atoms deviating by 0.043 Å and 0.041 Å from co-planarity. As with **Ni5**, the planes of the pyridine ring and the *N*-aryl plane are nearly perpendicular with a dihedral angle of 89.51°, as is commonly found for 2-(arylimino)pyridyl-nickel(II) halide structures reported elsewhere [23].

The ^{19}F NMR spectra of **Ni1**–**Ni5** all gave two closely located resonances for the *ortho*-4,4′-difluorobenzhydryl groups, which would suggest some restricted rotation in the CH(C$_6$H$_4$-F)$_a$(C$_6$H$_4$-F)$_b$ groups on account of the close proximity of the imine C-methyl group and the NiBr$_2$ unit. For **Ni4** and **Ni5**, additional resonances were seen for the *para*-F (δ -119.6 ppm) and *para*-OCF$_3$ (δ -57.8 ppm) groups. In the IR spectra of **Ni1**–**Ni5**,

bands typical of the (C=N) absorptions are seen around 1600 cm^{-1} which compares with 1644–1637 cm^{-1} in the free ligands, **L1**–**L5**.

2.2. Catalytic Evaluation for Ethylene Polymerization

2.2.1. Co-Catalyst Screening

To ascertain the most suitable activator, **Ni1** was employed as the test precatalyst and assessed with five different alkyl aluminum co-catalysts, including MAO (methylaluminoxane), MMAO (modified methylaluminoxane), $EtAlCl_2$, Et_2AlCl and EASC (ethylaluminium sesquichloride). All runs were performed in toluene under P_{C2H4} of 10 atm over 30 min with the temperature set at 30 °C (runs 1–5, Table 2). Inspection of the results indicated that all **Ni1**/co-catalyst combinations were effective in generating polyethylene, with activities spanning a fairly narrow range of 2.31–2.86 × 10^6 g of PE (mol of Ni)$^{-1}$ h^{-1} with the relative level falling in the order: $EtAlCl_2$ > EASC > Et_2AlCl > MMAO > MAO. With the aim to focus on just two types of co-catalyst, the most effective ethyl aluminum chlorides ($EtAlCl_2$) and aluminoxanes (MMAO) were selected for further optimization of the polymerization conditions.

Table 2. Assessment of the effectiveness of the co-catalyst using **Ni1** as precatalyst [a].

Run	Co-cat.	Al:Ni	Activity [b]	M_w [c]	M_w/M_n [c]	T_m (°C) [d]
1	EASC	400	2.71	3.70	2.27	57.5
2	Et_2AlCl	400	2.67	3.27	2.11	62.2
3	$EtAlCl_2$	400	2.86	4.76	2.56	68.8
4	MAO	2000	2.31	5.36	2.23	65.4
5	MMAO	2000	2.51	3.68	2.25	73.4

[a] Conditions: 2.0 µmol of **Ni1**, 100 mL of toluene, 10 atm C_2H_4, 30 °C, 30 min; [b] values in units of 10^6 g(PE)(mol Ni)$^{-1}$ h^{-1}; [c] M_w: kg·mol^{-1}, determined by GPC; [d] determined by DSC.

2.2.2. Ethylene Polymerization Using **Ni1**–**Ni5** in the Presence of $EtAlCl_2$

To achieve an effective set of polymerization conditions that could be employed to evaluate all five nickel precatalysts, **Ni1**/$EtAlCl_2$ was optimized by subjecting it to a systematic investigation examining Al:Ni molar ratio, reaction temperature and run time (Table 3). In the first instance, the Al:Ni molar ratio was modified between 300:1 and 600:1 with the temperature kept at 30 °C (runs 1–6, Table 3). Scrutiny of the results revealed the highest value of 3.20 × 10^6 g of PE (mol of Ni)$^{-1}$ h^{-1} was achieved at 500:1 (run 4, Table 3). At ratios in excess of 500:1, the activity decreased, as is demonstrated by the run performed at 600:1 that gave the lowest activity of 2.45 × 10^6 g of PE (mol of Ni)$^{-1}$ h^{-1} (run 6, Table 3). In terms of the polymer molecular weight, no dramatic variation could be identified with respect to changes in the molar ratio, though it could be viewed that some modest overall decline was evident with the M_w value dropping from 5.39 to 4.53 kg·mol^{-1} in line with the onset of chain transfer [33–48]. In any case, the polymer dispersity (M_w/M_n range: 2.56–2.88) remained narrow and unimodal, as shown in the GPC curves (Figure 4).

After that, we explored the influence of temperature on the performance of **Ni1**/$EtAlCl_2$ by varying it from 20 to 50 °C with the Al:Ni molar ratio maintained at 500:1 (runs 4, 7–9, Table 3). The highest activity of 3.20 × 10^6 g of PE (mol of Ni)$^{-1}$ h^{-1} was obtained at 30 °C, while further increasing the temperature saw the activity rapidly decline, reaching a low point of 5.0 × 10^5 g of PE (mol of Ni)$^{-1}$ h^{-1} at 50 °C (run 9, Table 3). Such a downward trend in activity can be interpreted in terms of deactivation of the active species and the lower solubility of ethylene at elevated temperature [24,29–50]. With respect to the resulting polymer, lower run temperature led to higher molecular weight PE (M_w = 9.59 kg·mol^{-1} at 20 °C) with a relatively high melting temperature (T_m = 102.1 °C). By comparison, with the run temperature at 50 °C, the molecular weight and melting point of the polymer dropped to their lowest values of 2.63 kg·mol^{-1} and 58.5 °C, respectively (run 9, Table 3). It is assumed that higher temperature increases the rate of chain termination compared to chain propagation, resulting in lower molecular weight PE [51]. Furthermore, the polymer dispersity remained narrow (M_w/M_n range: 2.2–3.0) and unimodal at the various

temperatures in accordance with the single-site nature of the catalyst (Figure 5). As a final remark, the appearance of the polymer visually changed from powder to wax due to its lower melting temperature (T_m range: 58.5–102.1 °C), lower molecular weight and likely higher branching content (*vide infra*).

Table 3. Polymerization results using **Ni1–Ni5** and $EtAlCl_2$ [a].

Run	Precat.	T (°C)	t (min)	Al:Ni	Activity [b]	M_w [c]	M_w/M_n [c]	T_m (°C) [d]
1	**Ni1**	30	30	300	1.37	5.22	2.68	67.4
2	**Ni1**	30	30	400	2.86	4.76	2.56	68.8
3	**Ni1**	30	30	450	3.10	4.84	2.88	69.8
4	**Ni1**	30	30	500	3.20	5.39	2.65	67.8
5	**Ni1**	30	30	550	2.65	4.53	2.64	66.1
6	**Ni1**	30	30	600	2.45	4.79	2.70	66.3
7	**Ni1**	20	30	500	2.76	9.59	3.02	102.1
8	**Ni1**	40	30	500	2.23	3.46	2.57	58.2
9	**Ni1**	50	30	500	0.50	2.63	2.21	57.4
10	**Ni1**	30	05	500	2.81	4.27	2.18	63.9
11	**Ni1**	30	15	500	3.02	4.97	2.69	72.1
12	**Ni1**	30	45	500	3.06	5.74	3.42	68.4
13	**Ni1**	30	60	500	2.74	6.18	3.43	68.9
14 [e]	**Ni1**	30	30	500	1.14	3.98	2.25	58.0
15 [f]	**Ni1**	30	30	500	trace	-	-	-
16	**Ni2**	30	30	500	2.88	4.61	2.89	68.3
17	**Ni3**	30	30	500	3.53	4.85	2.53	70.1
18	**Ni4**	30	30	500	3.87	5.83	2.90	68.1
19	**Ni5**	30	30	500	4.28	5.41	2.73	77.3

[a] Conditions: 2.0 µmol **Ni**, 100 mL toluene, 10 atm of C_2H_4. [b] 10^6g of PE (mol of Ni)$^{-1}$ h^{-1}. [c] M_w: kg·mol^{-1}, determined by GPC. [d] Determined by DSC. [e] 5 atm of C_2H_4. [f] 1 atm of C_2H_4.

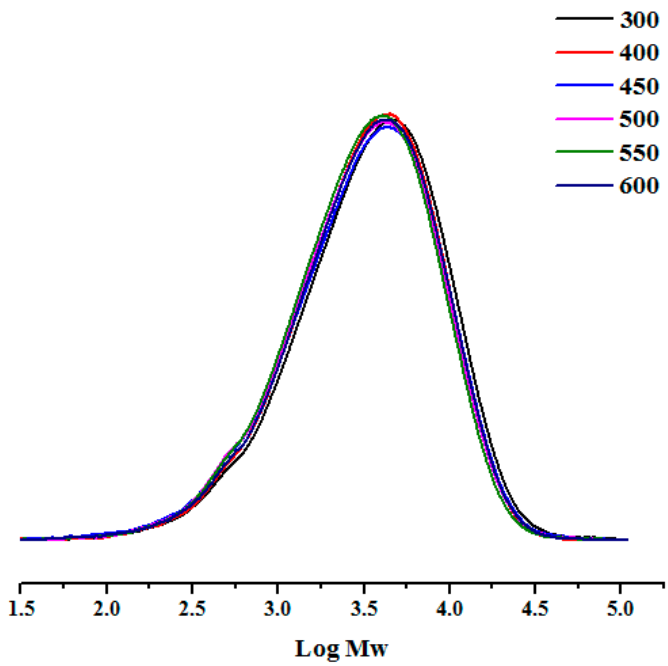

Figure 4. GPC curves of the PE produced using **Ni1**/$EtAlCl_2$ at different Al:Ni molar ratios (runs 1–6, Table 3).

To gauge the effectiveness of **Ni1**/$EtAlCl_2$ over time, the polymerization tests were conducted at various intervals between 5 and 60 min at 30 °C with the Al:Ni molar ratio fixed at 500:1 (runs 4, 10–13, Table 3). As a key observation, the catalytic activity displayed a modest upward trend in the first 30 min, culminating in a maximum activity of 3.20 × 10^6 g

of PE (mol of Ni)$^{-1}$ h^{-1} (run 4, Table 3). However, over the following 30 min the activity then gradually dropped to lower levels. It would seem likely that this decline in activity is attributable to the mass transfer limitations or to partial deactivation of the active species [52]. On the other hand, the molecular weight of the polymer increased and reached a maximum of 6.18 kg·mol^{-1} after 1 h, while the melting temperature of the polymer remained in a similar range (T_m range: 63.9–68.9 °C). As for the polymer dispersity, this remained narrow (M_w/M_n range: 2.6–2.9) and unimodal as is depicted in the GPC curves (Figure 6). As a final point, the catalytic activity of **Ni1**/EtAlCl$_2$ was also affected by ethylene pressure, with much lower activity observed at 5 atm, whereas at 1 atm only a trace amount of polymer was obtained (runs 14, 15, Table 3).

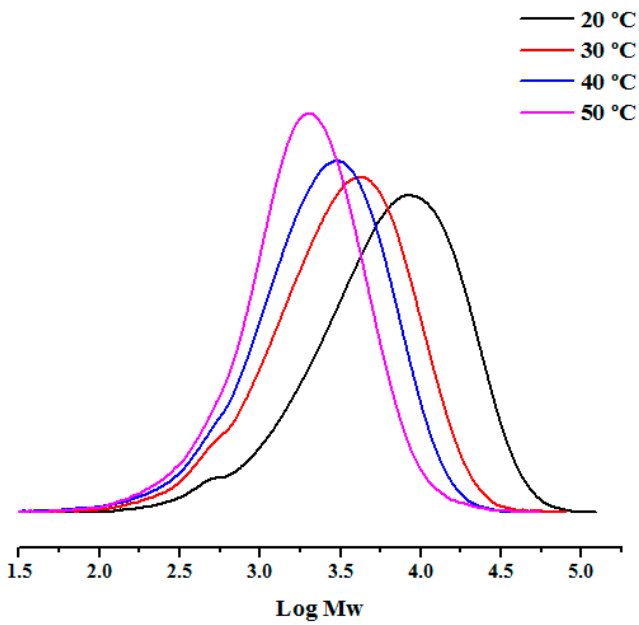

Figure 5. GPC curves of the PE produced using **Ni1**/EtAlCl$_2$ at different reaction temperatures (runs 4, 7–9, Table 3).

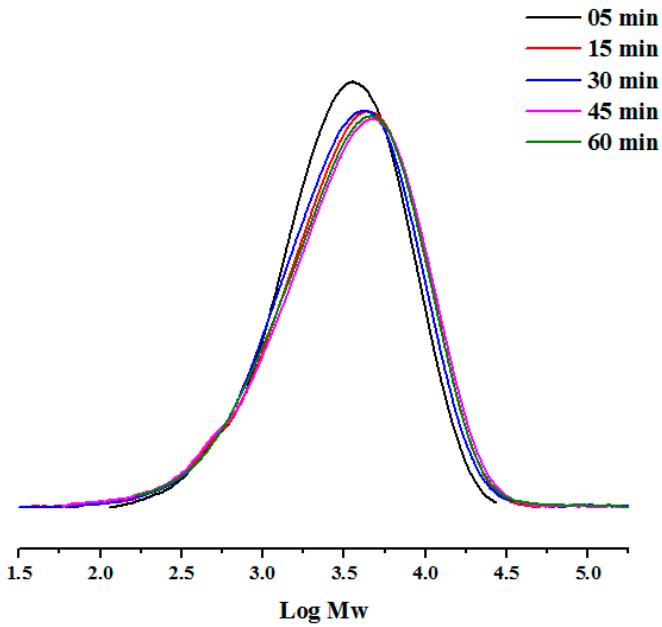

Figure 6. GPC curves of the PE produced using **Ni1**/EtAlCl$_2$ at different reaction times (runs 4, 10–13, Table 3).

Following the optimization studies performed on **Ni1**/$EtAlCl_2$, the most effective conditions were established as Al:Ni molar ratio = 500:1, reaction temp. = 30 °C and run time = 30 min. By employing these conditions, the remaining precatalysts were assessed with $EtAlCl_2$ as co-catalyst. As a general point, all precatalysts showed high activities ranging between 4.28 and 2.88 × 10^6 g of PE (mol of Ni)$^{-1}$ h^{-1} (runs 16–19, Table 3) with the relative order being: **Ni5** > **Ni4** > **Ni3** > **Ni1** > **Ni2**. Significantly, the precatalysts bearing electron withdrawing *para*-R substituents displayed a positive effect on catalytic activity. For example, when R = OCF_3 (**Ni5**), the activity of 4.28 × 10^6 g of PE (mol of Ni)$^{-1}$ h^{-1} was higher than that observed for R = Me (**Ni1**) of 3.20 × 10^6 g of PE (mol of Ni)$^{-1}$ h^{-1}. The explanation for this observation would likely stem from the increased electrophilicity of the metal center caused by the electron-withdrawing substituent which in turn increases the rate of ethylene insertion and higher activities [42–48]. Similar conclusions have been drawn from computational calculations that reveal favorable electronic effects of F or OCF_3 substitution on the net charge of the active species [53,54]. In terms of the polymer molecular weight, all polymers displayed low molecular weight in the range 4.61–5.83 kg·mol^{-1}, with no clear correlations with the *para*-R group evident. Nonetheless, all catalysts formed narrowly dispersed PE (M_w/M_n range: 2.5–2.9) (Figure 7), findings that are characteristic of single-site active center.

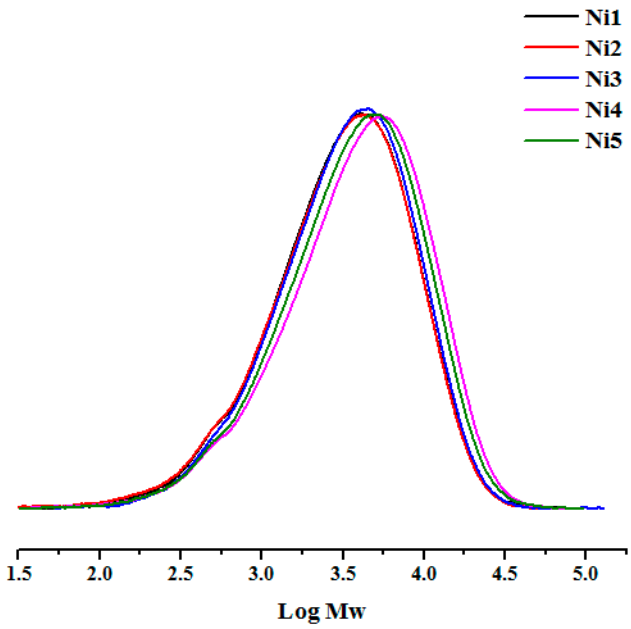

Figure 7. GPC curves of the PE produced using **Ni1–Ni5** in combination with $EtAlCl_2$ under optimized conditions (runs 4, 16–19, Table 3).

2.2.3. Ethylene Polymerization Using **Ni1**–**Ni5** in the Presence of MMAO

With MMAO now utilized as the co-catalyst, **Ni1** was again initially deployed to probe the effect of Al:Ni molar ratio, run temperature, run time and ethylene pressure. First the Al:Ni molar ratio was evaluated at 30 °C by varying it between 1500:1 and 3500:1 (runs 1–5, Table 4). From the data, it was evident that at 2000:1, the catalytic activity reached a peak value of 2.51 × 10^6 g PE (mol of Ni)$^{-1}$ h^{-1} (run 2, Table 4), which then gradually dropped as the ratio was increased beyond 2000:1 (runs 3–5, Table 4). On the other hand, the molecular weight of the PE gradually decreased from the outset, which can be related to the higher rates of chain transfer as compared to chain propagation at higher molar ratios of co-catalyst [52]. As has been noted throughout this study, the polymerizations are well-controlled with their dispersities (M_w/M_n), falling in this case between 2.21 and 2.54 (see Figure S1 for the GPC curves).

Table 4. Polymerization results using **Ni1–Ni5** and MMAO [a].

Run	Precat.	T (°C)	t (min)	Al:Ni	Activity [b]	M_w [c]	M_w/M_n [c]	T_m (°C) [d]
1	**Ni1**	30	30	1500	0.70	4.14	2.21	79.1
2	**Ni1**	30	30	2000	2.51	3.68	2.25	73.4
3	**Ni1**	30	30	2500	2.40	3.50	2.24	72.1
4	**Ni1**	30	30	3000	2.00	3.59	2.37	69.8
5	**Ni1**	30	30	3500	1.86	3.72	2.25	74.9
6	**Ni1**	20	30	2000	2.07	7.32	2.63	102.8
7	**Ni1**	40	30	2000	1.18	2.62	2.26	63.1
8	**Ni1**	50	30	2000	0.30	2.50	2.03	58.4
9	**Ni1**	30	05	2000	1.87	3.30	2.02	69.1
10	**Ni1**	30	15	2000	2.40	3.55	2.27	71.3
11	**Ni1**	30	45	2000	1.76	3.73	2.19	76.6
12	**Ni1**	30	60	2000	1.52	3.75	2.40	73.5
13 [e]	**Ni1**	30	30	2000	1.01	2.92	2.01	58.5
14 [f]	**Ni1**	30	30	2000	trace	-	-	-
15	**Ni2**	30	30	2000	2.05	3.69	2.28	74.5
16	**Ni3**	30	30	2000	2.62	3.49	2.36	74.4
17	**Ni4**	30	30	2000	2.84	3.98	2.38	72.5
18	**Ni5**	30	30	2000	3.15	3.83	2.38	77.4

[a] Conditions: 2.0 µmol **Ni**, 100 mL toluene, 10 atm of C_2H_4. [b] 10^6g of PE (mol of Ni)$^{-1}$ h^{-1}. [c] M_w: kg·mol^{-1}, determined by GPC. [d] Determined by DSC. [e] 5 atm of C_2H_4. [f] 1 atm of C_2H_4.

Next, with the Al:Ni molar ratio retained at 2000:1, the influence of the run temperature on the performance of **Ni1**/MMAO was investigated by performing the polymerizations between 20 and 50 °C (runs 2, 6–8, Table 4). As with $EtAlCl_2$ study, the results showed that the optimum temperature was at 30 °C (run 4, Table 4), above which deactivation of the active species occurred, leading to a rapid decrease in performance (e.g., 3.0 × 10^5 g PE (mol of Ni)$^{-1}$ h^{-1} at 50 ºC, run 8, Table 4); the lower concentration of ethylene at elevated temperature could also be a contributing factor [19–23,30–51]. The molecular weight of the PE also decreased from 7.32 to 2.50 kg·mol^{-1} (runs 2, 6–8, Table 4), which can be ascribed to a higher rate of chain termination when compared to chain propagation at elevated reaction temperature [17,45–49,55]. Nonetheless, the single site nature of the catalyst was maintained across the temperature range with narrow dispersities seen in all cases (M_w/M_n range: 2.63–2.03, see Figure S2). The melting temperatures (T_m) of the polymers displayed similar trends to those observed for **Ni1**/$EtAlCl_2$ with values dropping as the temperature was raised.

The time/activity profile of **Ni1**/MMAO was then investigated over various run times, typically 5, 15, 45, and 60 min with the Al:Ni molar ratio fixed at 2000:1 and the run temperature at 30 °C (runs 2, 9–12, Table 4). Similar to that seen with **Ni1**/$EtAlCl_2$, the catalytic activity reached a maximum after 30 min, in this case attaining a slightly lower value of 2.51 × 10^6 g of PE (mol of Ni)$^{-1}$ h^{-1} (run 2, Table 4). Likewise, the molecular weight of the polymer displayed an upward trend over time (from 3.30 kg·mol^{-1} after 5 min to 3.75 kg·mol^{-1} after 1 h), though less pronounced than that seen with **Ni1**/$EtAlCl_2$. As would be expected, the melting points of the polymers remained almost constant over the different run times (T_m range: 69.1–76.6 °C) and the dispersities narrowed (M_w/M_n range: 2.0–2.6). The effect of varying ethylene pressure mirrored that seen with $EtAlCl_2$, with catalytic activity and polymer molecular weight dropping as the pressure was reduced (runs 4, 14, 15, Table 4).

On the strength of the optimum conditions established for **Ni1**/$EtAlCl_2$, the four remaining nickel precatalysts **Ni2**–**Ni5** were similarly screened (Al:Ni molar ratio = 2000:1, reaction temp. = 30 °C and run time = 30 min); the results are collected in Table 4, runs 15–18. In general, comparable trends were found to that seen with **Ni1**–**Ni5**/$EtAlCl_2$, though lower catalytic activities were apparent (3.15–2.05 × 10^6 g of PE (mol of Ni)$^{-1}$ h^{-1} (MMAO) vs. 4.28–2.88 × 10^6 g of PE (mol of Ni)$^{-1}$ h^{-1} ($EtAlCl_2$)), which highlights the im-

portant role played by the alkyl-aluminum activator. Moreover, lower amounts of $EtAlCl_2$ are required for the nickel catalyst to reach optimal performance.

2.2.4. Microstructural Studies of the Polyethylenes

On inspection of Tables 3 and 4, the melting points (T_m) for the polyethylenes obtained with either $EtAlCl_2$ or MMAO were found to fall in the range of 58.5–102.8 °C, values that reflect both their level of branching and molecular weight. To provide further insight into the microstructural properties of the PEs, the ^1H and ^{13}C NMR spectra were recorded for selected Pes, including those generated using **Ni1**/$EtAlCl_2$ at 20, 30 and 50 °C (runs 7, 4 and 9, Table 3) and **Ni1**/MMAO at 30 °C (run 2, Table 4).

The ^1H NMR spectra of the PEs obtained using **Ni1**/$EtAlCl_2$ at the three different temperatures, 20, 30 and 50 °C (runs 7, 4, 9, Table 3), displayed the presence of both vinyl and vinylene functional groups, with characteristic signals at δ 5.02 ppm (H_a) and 5.84 (H_b) for the –CH=CH_2 protons with an integral ratio of 2:1 along with a signal at δ 5.40 ppm (H_c/$H_{c'}$) for the –CH=CH– protons. On closer examination of the spectra, it was evident that the vinylene to vinyl ratio, (–CH=CH–):(–CH=CH_2), was greatly affected by the reaction temperature (Figure 8). In particular, on increasing the temperature from 20 to 50 °C, this ratio increased from 3.1:1 to 11.8:1, which suggests that raising the polymerization temperature increased the rate of alkene isomerization.

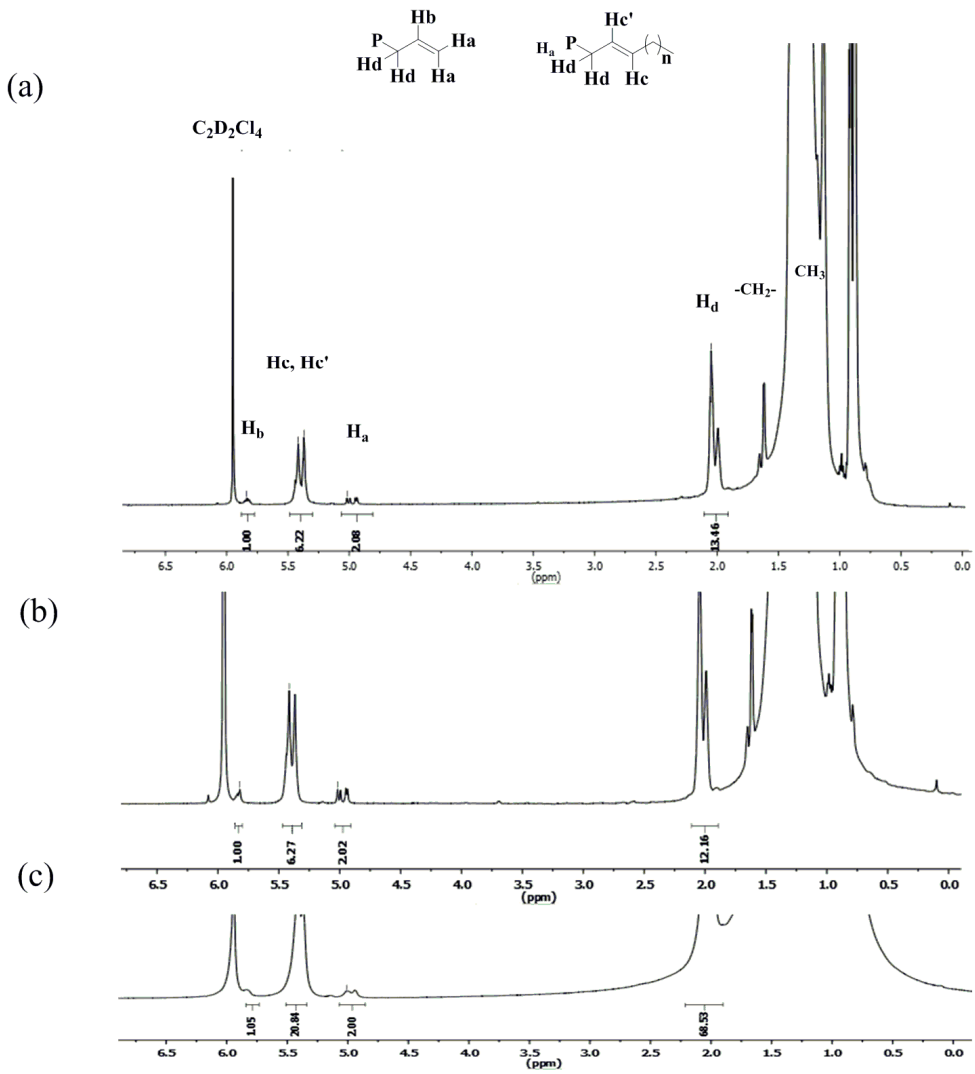

Figure 8. ^1H NMR spectra of the PE samples produced using **Ni1**/$EtAlCl_2$ at (**a**) 20 °C, (**b**) 30 °C and (**c**) 50 °C (runs 7, 4 and 9, Table 3); recorded at 100 °C in *d*-$C_2D_2Cl_4$.

In the ^{13}C NMR spectrum of the PE produced using **Ni1**/EtAlCl$_2$ at 20 °C (run 7, Table 3), characteristic resonances for the alkenic-carbons for the vinyl and vinylene functional groups, denoted C_a, C_b, C_c and $C_{c'}$, were seen in the downfield region (see inset in Figure S5). In the upfield region (main spectrum in Figure 9), peaks for the (–CH$_2$–) repeat unit along with less intense resonances corresponding to the various types of branch can be seen. Using approaches described in the literature [56–58], the assignment and relative percentage of each branch along with the branching density can be determined. Specifically, the analysis of this sample revealed 67 branches/1000 Cs, including methyl (76.3%), ethyl (1.6%), propyl (2.3%), butyl (4.8%), 1,4-paired methyl (2.5%), 1,6-paired methyl (2.9%) and longer chain branches (9.3%) (see Figure S5).

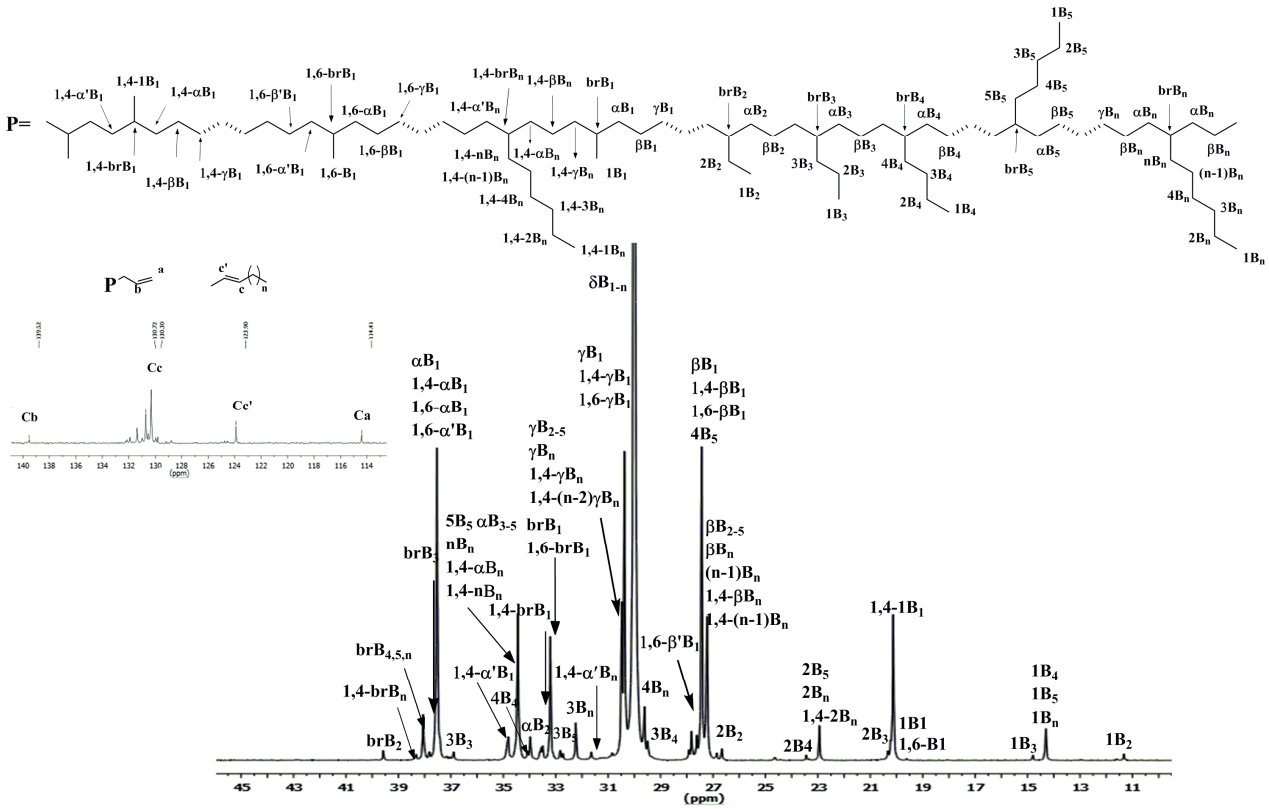

Figure 9. ^{13}C NMR spectrum of the PE produced using **Ni1**/EtAlCl$_2$ at 30 °C (run 4, Table 3) recorded at 100 °C in *d*-C$_2$D$_2$Cl$_4$.

By comparison, for the PE sample generated at 30 °C (run 4, Table 3), the number of branches increased to 91/1000 Cs, which included methyl (70.4%), ethyl (2.0%), propyl (2.9%), butyl (2.2%), 1,4-paired methyl (7.6%), 1,6-paired methyl (4.2%) and longer chain branches (10.3%) (see inset in Figure 9). This higher branching density was supported by a lower T_m value for this PE sample; similar results have been reported in the literature [23,59–61]. Conversely, the ^{13}C NMR spectrum of the PE generated at 50 °C (run 8, Table 3) showed the branching density increased to 135/1000 Cs and was based on methyl (25.8%), ethyl (4.8%), propyl (3.4%), butyl (8.1%), amyl (6.0%), 1,4-paired methyl (15.9%), 1,5-paired methyl (4.1%), 1,6-paired methyl (21.4%) and longer chain branches (10.1%) (see Figure S6).

To examine the effect of the co-catalyst on the microstructural properties of the polymer, the PE sample obtained using **Ni1**/MMAO at 30 °C (run 2, Table 4) was also characterized by ^{1}H and ^{13}C NMR spectroscopy. Interestingly, little difference in appearance of their spectra (see Figures S7 and S8, respectively) could be detected when compared with that obtained using **Ni1**/EtAlCl$_2$ at the same temperature. Indeed, the branching density was similar at 92 branches/1000 Cs, as was the branching composition: methyl (70.0%), ethyl

(3.0%), propyl (2.2%), butyl (1.6%), amyl (1.7%), 1,4-paired methyl (6.3%), 1,6-paired methyl (4.3%) and longer chain branches (10.5%).

2.2.5. Comparison between Current and Reported Analogues Precatalysts

With the intent to shed some light on the impact of the *ortho*-substituted 2,6-bis(4,4′-difluorobenzhydryl) groups as well as the variations in the electronic properties of the *para*-substituent on catalyst performance, the activity of **F** (**Ni5** in this work) and molecular weight of the polymer were compared with those of previously reported 2-iminopyridine-containing **C**, **D** and **E** (Figure 10); all polymerization runs were performed under optimized conditions of 10 atm of ethylene, 30 °C and with $EtAlCl_2$ as a co-catalyst [22,24–28]. As a notable observation, **F** displayed the highest activity of this series, which supports the view that the incorporation of an electron withdrawing OCF_3 group at the *para*-position has a positive effect on catalytic performance. Furthermore, **F** (**Ni4**) produced polymer with the highest molecular weight which highlights the beneficial role played by the 4,4′-difluorobenzhydryl groups at the *ortho* positions on chain propagation.

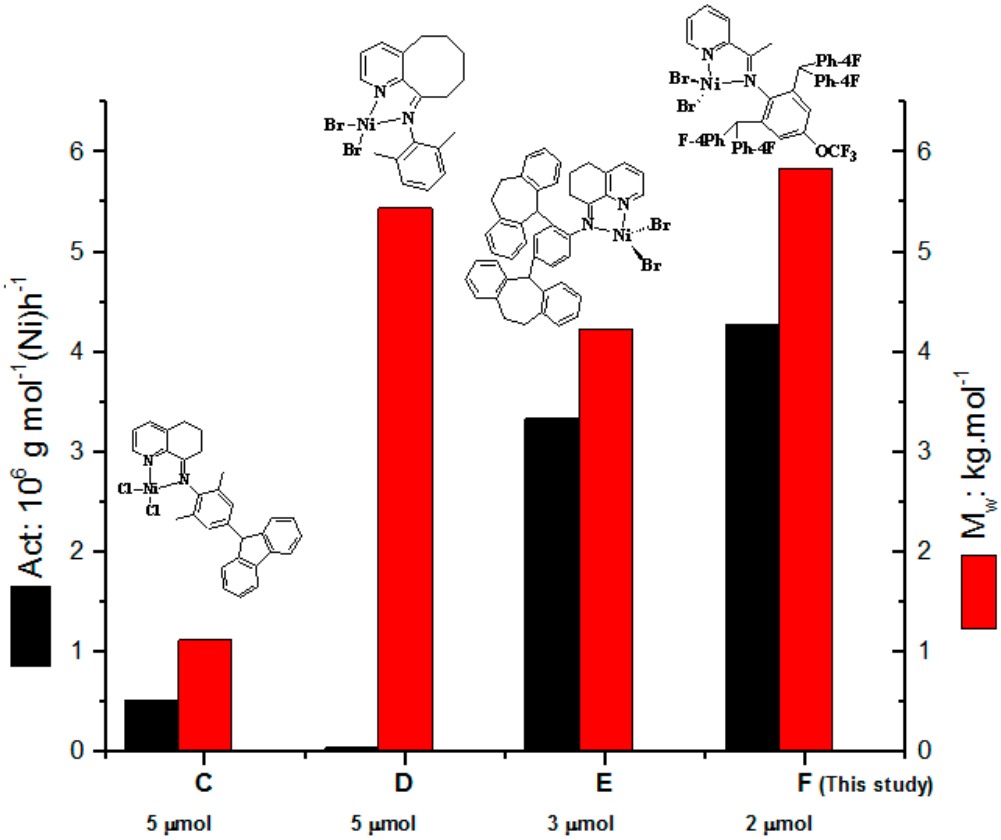

Figure 10. Comparison of **F** with previously reported non-fluorinated **C**, **D** and **E** under optimal conditions at 10 atm of C_2H_4.

3. Experimental Section

3.1. General Consideration

All manipulations of air or moisture-sensitive compounds were undertaken under an atmosphere of nitrogen using standard Schlenk techniques. The toluene used for the polymerization studies was dried over sodium for 8 h and distilled under a nitrogen atmosphere immediately prior to use. The ethylene monomer was purchased from Beijing Yanshan Petrochemical Company (Beijing, China) and utilized directly for the polymerization studies without any further purification. All other reagents were provided from Acros, Aldrich, or local suppliers. The co-catalysts MMAO (1.93 M solution in n-heptane) and MAO (methylaluminoxane, 1.30 M solution in toluene) were purchased from Anhui

Botai Electronic Materials Co., (Chuzhou, China) while $EtAlCl_2$ (ethylaluminumdichloride), Et_2AlCl (diethylaluminumchloride) and EASC (ethylaluminumsesquichloride, 40% solution in n-hexane) were provided by Yantai Lianli Chemical Co (Yantai, China). The NMR spectra were recorded on a Bruker AVANCE III (400 MHz instrument) (Bruker, Fällanden, Switzerland) using TMS as an internal standard at ambient temperature. In addition, ^{19}F NMR spectra of the ligands and nickel complexes were recorded on a Bruker AVANCE III 500 MHz instrument at ambient temperature. A Perkin Elmer System 2000 FT-IR spectrometer (Perkin-Elmer, Waltham, MA, USA) was used to record the FT-IR spectra, while elemental analysis was performed by a Flash EA1112 microanalyzer. Molecular weight (M_w) and molecular weight distributions (M_w/M_n) of the polyethylenes were determined with a PL-GPC220 instrument (Beijing, China) operating at 150 °C with 1,2,4-trichlorobenzene as eluting solvent. Differential scanning calorimetry (DSC, TA2000) (Perkin-Elmer, Waltham, MA, USA) was performed under a nitrogen atmosphere to record the melting temperatures of the polyethylenes. The temperature program was set as follows: a sample (4.0–6.0 mg) was heated to 130 °C at a heating rate of 20 °C per min and held for 5 min at the same temperature to remove its thermal history, then cooled to −50 °C at the same heating rate, held for 5 min at −50 °C and then heated to 130°C at a heating rate of 20 °C per min. A Bruker Avance III 500 MHz spectrometer was used to record the ^{13}C NMR spectra of the polyethylenes and these were run in a 5 mm standard glass tubes at 100 °C. The operating conditions used were as follows: spectral width 14.9701 kHz, acquisition time 2.1889 s, relaxation delay 1.0 s, number of scans at around 1024. Inverse gated ^{13}C NMR spectra were recorded at 110 °C on a Bruker Neo 700 NMR spectrometer equipped with a cryo BBO probe. Sample preparation involved dissolving 80–100 mg of polymer at 100 °C in 1,1,2,2-tetrachloroethane-d_2 (2 mL) containing TMS as an internal standard. The branching content of the polymer was calculated from the integration of the corresponding peaks in the ^{13}C NMR spectra according to literature approaches [59,60]. The anilines, 2,6-(bis(4,4′-difluorodibenzhydyl)-R-phenylamine (R = Me **A1**, Et **A2**, i-Pr **A3**, F **A4**, OCF_3 **A5**), were synthesized based on reported methods [45,61–63] and described in the SI.

*3.2. Synthesis of 2-{(2,6-(CH(C_6H_4-p-F)$_2$)$_2$-4-RC_6H_2)N=CMe}C_5H_4N (**L1** − **L5**)*

3.2.1. R = Me (**L1**)

A mixture of 2-acetylpyridine (0.25 g, 2.07 mmol) and $ZnCl_2$ (0.336 g, 2.5 mmol) in glacial acetic acid (3 mL) was stirred and heated to reflux for 20 min. Aniline **A1** (1.05 g, 2.07 mmol) was added to the reaction mixture and the stirring continued for a further 4 h at reflux. Once cooled to room temperature, a bright orange-red solid precipitated. The solid was filtered and washed with acetic acid (3 × 3 mL) and diethyl ether (5 × 6 mL) and then dried under reduced pressure to give the intermediate complex (**L1**)$ZnCl_2$ as a bright orange-red solid [64,65]. This solid was then dissolved in dichloromethane (3 mL) and demetallation of the zinc intermediate was undertaken by introducing 3 mL of aqueous potassium carbonate (0.553 g, 3.0 mmol) and vigorous stirring the reaction mixture for 1 h. The organic and aqueous phases were separated, and the organic layer washed with water (3 × 10 mL) and dried with $MgSO_4$. Following filtration, the solvent was removed under reduced pressure to afford the crude product which was then recrystallized from dichloromethane and *n*-hexane to afford **L1** as an orange powder (0.80 g, 65%). FT–IR (cm^{-1}): 2919 (w), 1858 (w), 1644 (m), 1600 (m), 1505 (s), 1465 (w), 1361 (w), 1301 (w), 1217 (s), 1157 (s), 1099 (w), 1038 (w), 1016 (w), 869 (w), 835 (s), 783 (m), 726 (w). ^1H NMR (400 MHz, $CDCl_3$, TMS): δ 8.60 (d, *J* = 6.40 Hz, 1H), 7.93 (d, *J* = 8.00 Hz, 1H), 7.72 (t, *J* = 8.0 Hz, 1H), 7.34 (t, *J* = 6.4 Hz, 1H), 6.86-6.96 (m, 16H), 6.61 (s, 2H), 5.20 (s, 2H), 2.18 (s, 3H), 1.20 (s, 3H). ^{13}C NMR (100 MHz, $CDCl_3$, TMS): 169.4, 162.6, 162.5, 160.2, 155.7, 148.6, 145.7, 139.1, 138.2, 138.1, 136.1, 132.0, 131.9, 131.0, 130.7, 130.6, 128.5, 124.8, 121.1, 115.3, 115.1, 114.9, 114.7, 50.5, 21.2, 17.0. ^{19}F NMR (470 MHz, $CDCl_3$): δ –116.29, –117.05. Anal. calcd for $C_{40}H_{30}F_4N_2$ (614.69): C, 88.16; H, 6.92; N, 4.56. Found: C, 87.76; H, 6.83; N, 4.59.

3.2.2. R = Et (**L2**)

By employing the same method and molar ratios as described for **L1**, **L2** was isolated as a yellow powder (0.92 g, 73%). FT-IR (cm^{-1}): 2962 (w), 2285 (w), 2082 (w), 1640 (m), 1600 (m), 1505 (m), 1460 (w), 1367 (w), 1301 (w), 1258 (s), 1215 (m), 1155 (w), 1013 (m), 873 (w), 788 (s), 731 (w), 667 (w). ^{1}H NMR (400 MHz, $CDCl_3$, TMS): δ 8.59 (d, *J* = 4.8 Hz, 1H), 7.96 (d, *J* = 7.8 Hz, 1H), 7.72 (t, *J* = 7.5 Hz, 1H), 7.35 (t, *J* = 5.4 Hz, 1H), 6.85-6.96 (m, 16H), 6.63 (s, 2H), 5.21 (s, 2H), 2.46 (q, *J* = 5.4 Hz, 2H), 1.19 (s, 3H), 1.05 (s, 3H). ^{13}C NMR (100 MHz, $CDCl_3$, TMS): 168.3, 162.0, 158.7, 154.6, 147.6, 144.9, 138.2, 138.1, 137.4, 137.1, 135.1, 130.9, 130.0, 129.9, 129.7, 129.6, 126.3, 123.8, 120.1, 114.3, 114.0, 113.9, 113.6, 49.5, 27.4, 16.0, 14.7. ^{19}F NMR (470 MHz, $CDCl_3$): δ −116.32, −117.14. Anal. calcd for $C_{41}H_{32}F_4N_2$ (628.71): C, 78.33; H, 5.13; N, 4.46. Found: C, 78.73; H, 5.15; N, 4.48.

3.2.3. R = i-Pr (**L3**)

By employing the same method and molar ratios as described for **L1**, **L3** was isolated as a yellow powder (0.88 g, 68%). FT-IR (cm^{-1}): 2959 (w), 2932 (w), 1973 (w), 1637 (C=N, m), 1599 (m), 1503 (s), 1464 (w), 1366 (w), 1301 (w), 1218 (s), 1155 (m), 1097 (m), 1015 (w), 832 (s), 782 (m), 729 (m), 664 (w). ^{1}H NMR (400 MHz, $CDCl_3$, TMS): δ 8.59 (d, *J* = 4.8 Hz, 1H), 7.97 (d, *J* = 8.0 Hz, 1H), 7.72 (t, *J* = 7.6 Hz, 1H), 7.35 (t, *J* = 5.2 Hz, 1H), 6.66-6.99 (m, 16H), 6.47 (s, 2H), 5.21 (s, 2H), 2.71 (m, 1H), 1.21 (s, 3H), 1.07 (d, *J* = 10.0 Hz, 6H). ^{13}C NMR (100 MHz, $CDCl_3$, TMS): δ 162.5, 160.2, 160.1, 155.7, 148.6, 145.9, 143.0, 139.2, 139.2, 138.2, 138.2, 136.1, 131.7, 131.0, 130.9, 130.7, 130.6, 125.9, 124.8, 121.1, 115.3, 115.1, 114.9, 114.6, 58.4, 50.6, 33.5, 24.0, 18.2, 17.1. ^{19}F NMR (470 MHz, $CDCl_3$): δ −116.35, −117.13. Anal. calcd for $C_{42}H_{34}F_4N_2$ (642.74): C, 78.49; H, 5.33; N, 4.36. Found: C, 78.03; H, 5.29; N, 4.32.

3.2.4. R = F (**L4**)

By employing the same method and molar ratios as described for **L1**, **L4** was isolated as a yellow powder (0.18 g, 75%). FT-IR (cm^{-1}): 3070 (w), 2962 (w), 2282 (w), 2110 (w), 1642 (C=N, m), 1599 (m), 1505 (s), 1466 (w), 1441 (m), 1363 (w), 1302 (m), 1259 (m), 1219 (s), 1155 (m), 1095 (m), 1016 (m), 873 (w), 760 (s), 748 (w), 722 (w), 681 (w). ^{1}H NMR (400 MHz, $CDCl_3$, TMS): δ 8.61 (d, *J* = 4.4 Hz, 1H), 7.94 (d, *J* = 7.6 Hz, 1H), 7.73 (t, *J* = 1.6 Hz, 1H), 7.37 (t, *J* = 1.6 Hz, 1H), 6.88-6.94 (m, 16H), 6.55 (d, *J* = 9.6 Hz, 2H), 5.21 (s, 2H), 1.20 (s, 3H). ^{13}C NMR (100 MHz, $CDCl_3$, TMS): δ 170.2, 162.8, 162.7, 160.3, 157.7, 155.4, 148.7, 144.1, 138.2, 137.4, 137.3, 136.2, 134.2, 134.1, 131.0, 130.9, 130.6, 130.5, 125.0, 121.1, 115.5, 115.3, 115.2, 114.9, 114.7, 50.5, 17.0. ^{19}F NMR (470 MHz, $CDCl_3$): δ −115.67, −116.41, −119.70. Anal. calcd for $C_{39}H_{27}F_5N_2$ (618.65): C, 75.72; H, 4.40; N, 4.53. Found: C, 75.42; H, 4.42; N, 4.55.

3.2.5. R = OCF_3 (**L5**)

By employing the same method and molar ratios as described for **L1**, **L5** was isolated as a yellow powder (1.10 g, 80%). FT-IR (cm^{-1}): 3044 (w), 2914 (w), 1892 (w), 1643 (C=N, m), 1602 (m), 1583 (w), 1567 (w), 1505 (s), 1465 (w), 1442 (m), 1366 (m), 1303 (w), 1254 (m), 1224 (w), 1209 (w), 1195 (w), 1172 (w), 1154 (w), 1098 (m), 1043 (w), 1014 (m), 993 (w), 875 (w), 833 (s), 794 (w), 783 (w), 740 (m), 656 (m). ^{1}H NMR (400 MHz, $CDCl_3$, TMS): δ 8.59 (d, *J* = 4.0 Hz, 1H), 7.93 (d, *J* = 7.6 Hz, 1H), 7.72 (t, *J* = 7.6 Hz, 1H), 7.35 (t, *J* = 6.4 Hz, 1H), 6.88–6.94 (m, 16H), 6.67 (s, 2H), 5.19 (s, 2H). ^{13}C NMR (100 MHz, $CDCl_3$, TMS): δ 160.3, 148.7, 146.7, 138.0, 137.1, 136.2, 134.0, 130.9, 130.8, 130.6, 130.5, 125.1, 121.1, 120.8, 115.6, 115.4, 115.2, 115.0, 50.5, 17.2. ^{19}F NMR (470 MHz, $CDCl_3$): δ –58.22, –115.53, –116.29. Anal. calcd for $C_{40}H_{27}F_7N_2O$ (684.66): C, 70.17; H, 3.98; N, 4.09. Found: C, 69.78; H, 4.01; N, 4.08.

*3.3. Synthesis of [2-{(2,6-(CH(C_6H_4-p-F)$_2$)$_2$-4-RC_6H_2)N=CMe}C_5H_4N]$NiBr_2$ (**Ni1** − **Ni5**)*

3.3.1. R = Me (**Ni1**)

Under a nitrogen atmosphere, **L1** (0.30 g, 0.52 mmol) and $NiBr_2$(DME) (0.08 g, 0.26 mmol) were added to a mixture of dichloromethane (10 mL) and ethanol (10 mL) and stirred for 12 h at room temperature. All the volatiles were then evaporated under reduced pressure

and diethyl ether added to the residue to induce precipitation. The precipitate was filtered, washed with diethyl ether (3 × 10 mL) and dried to afford **Ni1** as an orange powder (0.20 g, 58%). FT-IR (cm^{-1}): 3353 (w), 3063 (w), 2921 (w), 1630 (w), 1598 (C=N, m), 1571 (w), 1505 (s), 1450 (w), 1372 (w), 1318 (w), 1253 (w), 1221 (s), 1158 (s), 1097 (w), 1061 (w), 1021 (w), 982 (w), 837 (s), 783 (m), 727 (w). ^{19}F NMR (470 MHz, $CDCl_3$): δ −116.13, −117.52. Anal. calcd for $C_{40}H_{30}Br_2F_4N_2Ni$ (833.19): C, 57.66; H, 3.63; N, 3.36. Found: C, 57.63; H, 3.56; N, 3.57.

3.3.2. R = Et (**Ni2**)

By utilizing a similar procedure and molar ratios to those described for **Ni1**, **Ni2** was isolated as an orange powder (0.20 g, 63%). FT-IR (cm^{-1}): 3061 (w), 2970 (w), 2894 (w), 1627 (w), 1597 (m), 1571 (w), 1505 (s), 1455 (w), 1425 (w), 1373 (w), 1318 (w), 1220 (s), 1158 (m), 1095 (w), 1051 (w), 1020 (w), 878 (w), 836 (s), 783 (m), 726 (w). ^{19}F NMR (470 MHz, $CDCl_3$): δ −115.44, −116.82. Anal. calcd for $C_{41}H_{32}Br_2F_4N_2Ni$ (847.22): C, 58.13; H, 3.81; N, 3.31. Found: C, 58.02; H, 3.84; N, 3.34.

3.3.3. R = i-Pr (**Ni3**)

By utilizing a similar procedure and molar ratios to that described for **Ni1**, **Ni3** was isolated as an orange powder (0.22 g, 60%). FT-IR (cm^{-1}): 3063 (w), 2962 (w), 1598 (m), 1574 (w), 1505 (s), 1449 (w), 1372 (w), 1317 (w), 1256 (w), 1223 (s), 1158 (m), 1134 (w), 1097 (w), 1020 (w), 877 (w), 837 (s), 783 (m), 750 (w), 726 (w). ^{19}F NMR (470 MHz, $CDCl_3$): δ −115.45, −116.82. Anal. calcd for $C_{42}H_{34}Br_2F_4N_2Ni$ (861.24): C, 58.57; H, 3.98; N, 3.25. Found: C, 58.53; H, 4.03; N, 3.42.

3.3.4. R = F (**Ni4**)

By utilizing a similar procedure and molar ratios to that described for **Ni1**, **Ni4** was isolated as an orange powder (0.27 g, 77%). FT-IR (cm^{-1}): 3358 (w), 3070 (w), 1912 (w), 1630 (w), 1597 (C=N, m), 1574 (w), 1505 (s), 1448 (m), 1373 (w), 1320 (w), 1263 (w), 1224 (s), 1157 (w), 1100 (w), 1055 (w), 1007 (w), 942 (w), 869 (w), 839 (s), 781 (w), 725 (w), 684 (w), 651 (w). ^{19}F NMR (470 MHz, $CDCl_3$): δ −115.66, −116.41, −119.6. Anal. calcd for $C_{39}H_{27}Br_2F_5N_2Ni$ (837.15): C, 55.96; H, 3.25; N, 3.35. Found: C, 55.85; H, 3.18; N, 3.28.

3.3.5. R = OCF_3 (**Ni5**)

By utilizing a similar procedure and molar ratios to that described for **Ni1**, **Ni5** was isolated as an orange powder (0.36 g, 84%). FT-IR (cm^{-1}): 3761 (w), 3062 (w), 2161 (w), 2028 (w), 1971 (w), 1624 (w), 1598 (m), 1574 (w), 1505 (s), 1449 (w), 1373 (w), 1317 (w), 1263 (m), 1221 (s), 1190 (w), 1156 (m), 1098 (w), 1017 (w), 982 (w), 879 (w), 834 (s), 784 (m), 730 (w). ^{19}F NMR (470 MHz, $CDCl_3$): δ −57.84, −114.76, −115.72. Anal. calcd for $C_{40}H_{27}Br_2F_7N_2NiO$ (903.16): C, 53.20; H, 3.01; N, 3.10. Found: C, 53.06; H, 3.03; N, 2.89.

3.4. Ethylene Polymerization Evaluation

3.4.1. The Polymerizations at P_{C2H4} = 5 or 10 atm Were Performed in a Stainless Steel Autoclave (250 mL Capacity) Equipped with a Mechanical Stirrer and an Ethylene Pressure and Temperature Control System

The autoclave was evacuated and backfilled with nitrogen (×3) and once with ethylene (×1). The nickel precatalyst (Ni1–Ni5, 2.0 μmol) was dissolved in toluene (50 mL) and injected into the autoclave at the desired reaction temperature followed by freshly distilled toluene (25 mL). The required amounts of co-catalyst ($EtAlCl_2$, Et_2AlCl, EASC, MAO or MMAO) and toluene (50 mL), were successively injected using a syringe, taking the total volume to 100 mL. The autoclave was immediately pressurized to the required ethylene pressure (5 or 10 atm) with rapid stirring. After a predetermined reaction time, the flow of ethylene was stopped, and the reactor cooled in a water bath. Once the temperature had reached ambient, the reactor was vented, and the reactor opened. The resulting mixture was poured into a 10% solution of HCl in ethanol, filtered and washed with ethanol several times before drying under reduced pressure until of constant weight.

3.4.2. Polymerizations at P_{C2H4} = 1 atm

The Polymerizations at 1 atm were conducted in a schlenk vessel. The nickel precatalyst (0.002 mmol) was added to a Schlenk vessel equipped with a stir bar, followed by freshly distilled toluene (30 mL). The required amount of aluminum co-catalyst was then added by syringe. The reaction mixture was stirred at 1 atm of ethylene pressure at room temperature. After 30 min, the supply of ethylene was ceased, and the reaction vessel vented. Following the addition of 10% hydrochloric acid in ethanol, the polymer was filtered and washed with ethanol and then dried under reduced pressure until of constant mass.

3.5. X-ray Crystallographic Studies

Single crystals of **Ni4′** and **Ni5** suitable for an X-ray diffraction determination were grown by slow diffusion of diethyl ether into the corresponding dichloromethane solutions at room temperature. Data collection was performed on a Rigaku Saturn724+ CCD with graphite-monochromatic Cu-Kα radiation (λ = 1.54184 Å) at 169(2) K. The cell parameters were obtained by global refinement of the positions of all collected reflections. Intensities were corrected for Lorentz and polarization effects and empirical absorption. The structures were solved by applying direct methods and refined by full-matrix least-squares on F^2. All hydrogen atoms were placed in the calculated positions. Structure solution and refinement were performed using the Olex2 1.2 package [66]. The structure was solved with the SHELXT [67] and structure solution program using Intrinsic Phasing and refinement with the SHELXL [68] refinement package using Least Squares minimization. Crystal data and structure refinements for **Ni4′** and **Ni5** are provided in Table S1.

4. Conclusions

A series of novel 2-(2,6-bis(bis(4,4′-difluorobenzhydryl)-4-R-phenylimino)ethyl) pyridines (R = Me (**L1**), Et (**L2**), *i*-Pr (**L3**), F (**L4**), OCF_3 (**L5**), together with their corresponding $LNiBr_2$ complexes, **Ni1–Ni5**, were successfully prepared and fully characterized by a range of techniques, including FT-IR, ^{1}H, ^{19}F, ^{13}C NMR spectroscopy and elemental analysis. In addition, structural characterization of **Ni5** and a derivative of **Ni4**, $(\mathbf{L4})_2NiBr_2$ (**Ni4′**), was undertaken. Following an initial screen of a range of aluminum-alkyl co-catalysts, $EtAlCl_2$ and MMAO were taken forward to investigate the effects of the *para*-R substitution on ethylene polymerization. All the catalysts exhibited high activity in the range of 0.50 to 4.28 × 10^6 g of PE (mol of Ni)$^{-1}$ h^{-1} ($EtAlCl_2$) and 0.30 to 3.15 × 10^6 g of PE (mol of Ni)$^{-1}$ h^{-1} (MMAO), generating highly branched PE with low molecular weight and narrow dispersity, along with a high content of unsaturated end groups (ratio of vinylene to vinyl, range: 3.1:1–10.3.1). Significantly, catalysts bearing electron withdrawing 4-substituents (e.g., F and OCF_3) showed higher activities than their electron donating counterparts. Furthermore, the catalytic activity, type of polymer unsaturation, molecular weight and branching densities were greatly influenced by the reaction temperature. Finally, by comparison with a series of structurally related nickel catalysts, the effect of *para*-OCF_3 substitution was to enhance catalytic activity, while the *ortho*-4,4′-difluorobenzhydryl groups augmented polymer molecular weight.

Supplementary Materials: The following are available online at https://www.mdpi.com/article/10.3390/catal12121520/s1, Synthesis of the organic compounds **A1**–**A5** as ligands according to literature [62,63] and characterization, ^{19}F NMR of ligands and complexes, the GPC curves of the polyethylene samples produced with the **Ni1**/MMAO, ^{13}C NMR and ^{1}H NMR spectra of the polyethylene samples generated using **Ni1**/MAO and **Ni1**/$EtAlCl_2$ (PDF). In addition, crystallographic information for **Ni4′** (CCDC 2215182) and **Ni5** (CCDC 2215183) (CIF) are provided in the supporting information. Scheme S1 Synthetic route to **A1**–**A5**; Figure S1 GPC curves for the polyethylene produced using **Ni1**/MMAO at different Al:Ni molar ratios (runs 1–5, Table 4); Figure S2 GPC curves for the polyethylene produced using **Ni1**/MMAO, at different reaction temperatures (runs 2, 6–8, Table 4); Figure S3 GPC curves for the polyethylene produced using **Ni1**/MMAO at different reaction times (runs 2, 9–12, Table 4); Figure S4 GPC curves for the polyethylene produced using

Ni1–**Ni5**/MMAO under optimized conditions (runs 2, 15–18, Table 4); Figure S5 13C NMR spectrum of the polyethylene sample produced using **Ni1**/EtAlCl2 at 20 °C (run 7, Table 3), including an inset of the alkenic region and a segment of the assigned polymer backbone; recorded at 100 °C in d-C2D2Cl4; Figure S6 13C NMR spectrum of the polyethylene sample produced using **Ni1**/EtAlCl2 at 50 °C (run 9, Table 3), including an inset of the alkenic region and a segment of the assigned polymer backbone; recorded at 100 °C in d-C2D2Cl4; Figure S7 1H NMR spectrum of the polyethylene sample produced using **Ni1**/MMAO at 30 °C (run 2, Table 4); recorded at 100 °C in d-C2D2Cl4; Figure S8 13C NMR spectrum of the polyethylene sample produced using **Ni1**/MMAO at 30 °C (run 2, Table 4), including an inset of the alkenic region and a segment of the assigned polymer backbone; recorded at 100 °C in d-C2D2Cl4; Figures S9–S18 19F NMR spectrum of **L1**, **L2**, **L3**, **L4**, **L5**, **Ni1**, **Ni2**, **Ni3**, **Ni4**, **Ni5** (recorded in CDCl3 at room temperature); Figure S19 DSC curve **Ni**/MMAO (recorded at room temperature); Table S1 Crystal data and structure refinement for **Ni4′** and **Ni5**.

Author Contributions: Design of the study by W.-H.S.; synthesis of the organic compounds and the nickel complexes by Z.H.; characterization by Z.H and W.-H.S.; X-ray study by M.L., Q.Z. and T.L.; catalytic study by Z.H.; characterization of polyethylene by Z.H.; writing and editing Z.H., G.A.S., Y.M. and W.-H.S. All authors have read and agreed to the published version of the manuscript.

Funding: This research was funded by the National Natural Science Foundation of China (21871275).

Data Availability Statement: The data of this manuscript are available from the corresponding authors upon request.

Acknowledgments: Z.H. is grateful to the Chinese Academy of Sciences President's International Fellowship Initiative (no. 2020PM0055). G.A.S. thanks the Chinese Academy of Sciences for a President's International Fellowship for Visiting Scientists.

Conflicts of Interest: The authors declare no conflict of interest.

References

1. Soshnikov, I.E.; Semikolenova, N.V.; Bryliakov, K.P.; Antonov, A.A.; Sun, W.-H.; Talsi, E.P. The nature of nickel species formed upon the activation of α-diimine nickel (II) pre-catalyst with alkylaluminum sesquichlorides. *J. Organomet. Chem.* **2020**, *907*, 121063. [CrossRef]
2. Killian, C.M.; Tempel, D.J.; Johnson, L.K.; Brookhart, M. Living polymerization of α-olefins using Ni(II)−α-diimine catalysts. Synthesis of new block polymers based on α-olefins. *J. Am. Chem. Soc.* **1996**, *118*, 11664–11665. [CrossRef]
3. Johnson, L.K.; Killian, C.M.; Brookhart, M. New Pd (II)-and Ni (II)-based catalysts for polymerization of ethylene and alpha-olefins. *J. Am. Chem. Soc.* **1995**, *117*, 6414–6415. [CrossRef]
4. Ittel, S.D.; Johnson, L.K.; Brookhart, M. Late-metal catalysts for ethylene homo- and copolymerization. *Chem. Rev.* **2000**, *100*, 1169–1204. [CrossRef] [PubMed]
5. Britovsek, G.J.; Gibson, V.C.; Hoarau, O.D.; Spitzmesser, S.K.; White, A.J.; Williams, D.J. Iron and cobalt ethylene polymerization catalysts: Variations on the central donor. *Inorg. Chem.* **2003**, *42*, 3454–3465. [CrossRef]
6. Sun, W.-H.; Zhang, S.; Zuo, W. Our variations on iron and cobalt catalysts toward ethylene oligomerization and polymerization. *Comptes Rendus Chim.* **2008**, *11*, 307–316. [CrossRef]
7. Allen, K.E.; Campos, J.S.; Daugulis, O.; Brookhart, M. Living polymerization of ethylene and copolymerization of ethylene/methyl acrylate using "sandwich" diimine palladium catalysts. *ACS Catal.* **2015**, *5*, 456–464. [CrossRef]
8. Wang, Z.; Liu, Q.; Solan, G.A.; Sun, W.-H. Recent advances in Ni-mediated ethylene chain growth: Nimine-donor ligand effects on catalytic activity, thermal stability and oligo-/polymer structure. *Coord. Chem. Rev.* **2017**, *350*, 68–83. [CrossRef]
9. Wang, Z.; Solan, G.A.; Zhang, W.; Sun, W.-H. Carbocyclic-fused N,N,N-pincer ligands as ring-strain adjustable supports for iron and cobalt catalysts in ethylene oligo-/polymerization. *Coord. Chem. Rev.* **2018**, *363*, 92–108. [CrossRef]
10. Nakamura, A.; Ito, S.; Nozaki, K. Coordination—Insertion copolymerization of fundamental polar monomers. *Chem. Rev.* **2009**, *109*, 5215–5244. [CrossRef]
11. Carrow, B.P.; Nozaki, K. Transition-metal-catalyzed functional polyolefin synthesis: Effecting control through chelating ancillary ligand design and mechanistic insights. *Macromolecules* **2014**, *47*, 2541–2555. [CrossRef]
12. Mu, H.; Pan, L.; Song, D.; Li, Y. Neutral nickel catalysts for olefin homo-and copolymerization: Relationships between catalyst structures and catalytic properties. *Chem. Rev.* **2015**, *115*, 12091–12137. [CrossRef]
13. Chen, Z.; Brookhart, M. Exploring ethylene/polar vinyl monomer copolymerizations using Ni and Pd α-diimine catalysts. *Acc. Chem. Res.* **2018**, *51*, 1831–1839. [CrossRef]
14. D'Auria, I.; Saki, Z.; Liu, M.; Sun, W.-H.; Pellecchia, C. Copolymerization of ethylene and methyl acrylate by dibenzocycloheptyl-substituted aryliminopyridyl Ni(II) catalysts. *Macromol* **2022**, *2*, 500–508. [CrossRef]
15. Cotts, P.M.; Guan, Z.; McCord, E.; McLain, S. Novel branching topology in polyethylenes as revealed by light scattering and ^{13}C NMR. *Macromolecules* **2000**, *33*, 6945–6952. [CrossRef]

16. Guan, Z.; Cotts, P.; McCord, E.; McLain, S. Chain walking: A new strategy to control polymer topology. *Science* **1999**, *283*, 2059–2062. [CrossRef]
17. Zeng, Y.; Mahmood, Q.; Liang, T.; Sun, W.H. Judiciously balancing steric and electronic influences on 2,3-diiminobutane- based Pd (II) complexes in nourishing polyethylene properties. *J. Polym. Sci. Part A-1 Polym. Chem.* **2017**, *55*, 3214–3222. [CrossRef]
18. Sage, D.D.; Zhang, Q.; Liu, M.; Solan, G.A.; Sun, Y.; Sun, W.-H. LLDPE-like polymers accessible via ethylene homopolymerization using nitro-appended 2-(arylimino)pyridine-nickel catalysts. *Catalysts* **2022**, *12*, e961. [CrossRef]
19. Gibson, V.C.; Redshaw, C.; Solan, G.A. Bis(imino)pyridines: Surprisingly reactive ligands and a gateway to new families of catalysts. *Chem. Rev.* **2007**, *107*, 1745–1776. [CrossRef]
20. Zhang, W.; Sun, W.-H.; Redshaw, C. Tailoring iron complexes for ethylene oligomerization and/or polymerization. *Dalton Trans.* **2013**, *42*, 8988–8997. [CrossRef]
21. Suo, H.; Solan, G.A.; Ma, Y.; Sun, W.-H. Developments in compartmentalized bimetallic transition metal ethylene polymerization catalysts. *Coord. Chem. Rev.* **2018**, *372*, 101–116. [CrossRef]
22. Laine, T.V.; Piironen, U.; Lappalainen, K.; Klinga, M.; Aitola, E.; Leskelä, M. Pyridinylimine-based nickel (II) and palladium (II) complexes: Preparation, structural characterization and use as alkene polymerization catalysts. *J. Organomet. Chem.* **2000**, *606*, 112–124. [CrossRef]
23. Guo, J.; Zhang, W.; Mahmood, Q.; Zhang, R.; Sun, Y.; Sun, W.H. Vinyl/Vinylene functionalized highly branched polyethylene waxes obtained using electronically controlled cyclohexyl-fused pyridinylimine-nickel precatalysts. *J. Polym. Sci. A Polym Chem.* **2018**, *56*, 1269–1281. [CrossRef]
24. Jiang, S.; Zheng, Y.; Liu, M.; Yu, Z.; Ma, Y.; Solan, G.A.; Zhang, W.; Liang, T.; Sun, W.-H. Polyethylene Waxes with Short Chain Branching via Steric and ElectronicTuningofan8-(Arylimino)-5,6,7-trihydroquinoline-nickel. *Organometallics* **2022**, *43*, 227–230.
25. Liu, M.; Zhang, R.; Ma, Y.; Han, M.; Solan, G.A.; Yang, W.; Liang, T.; Sun, W.-H. Trifluoromethoxy-substituted nickel catalysts for producing highly branched polyethylenes: Impact of solvent, activator and N,N′-ligand on polymer properties. *Polym. Chem.* **2022**, *13*, 1040–1058. [CrossRef]
26. Zhang, Q.; Lin, W.; Liu, T.; Ye, Z.; Liang, T.; Sun, W.-H. Fluorinated Sterically Bulky Mononuclear and Binuclear 2-Iminopyridylnickel Halides for Ethylene Polymerization: Effects of Ligand Frameworks and Remote Substituents. *ACS Omega* **2021**, *6*, 30157–30172. [CrossRef]
27. Wang, Z.; Zhang, Y.; Ma, Y.; Hu, X.; Solan, G.A.; Sun, Y.; Sun, W.H. Molecular weight control of polyethylene waxes using a constrained imino-cyclopenta[*b*]pyridyl-nickel catalyst. *J. Polym. Sci. A Polym. Chem.* **2017**, *55*, 3494–3505. [CrossRef]
28. Huang, C.; Zeng, Y.; Flisak, Z.; Zhao, Z.; Liang, T.; Sun, W.H. Tailoring polymers through interplay of ligands within precatalysts: 8-(Nitro/benzhydryl-arylimino)-7,7-dimethyl-5,6-dihydroquinolylnickel halides in ethylene polymerization. *J. Polym. Sci. A Polym. Chem.* **2017**, *55*, 2071–2083. [CrossRef]
29. Zhang, L.; Hao, X.; Sun, W.-H.; Redshaw, C. Synthesis, characterization, and ethylene polymerization behavior of 8-(nitroarylamino)-5, 6, 7-trihydroquinolylnickel dichlorides: Influence of the nitro group and impurities on catalytic activity. *ACS Catal.* **2011**, *1*, 1213–1220. [CrossRef]
30. Leroux, F.R.; Manteau, B.; Vors, J.-P.; Pazenok, S. Trifluoromethyl ethers–synthesis and properties of an unusual substituent. *Beilstein J. Org. Chem.* **2008**, *4*, 13–23. [CrossRef]
31. Huang, Z.; Song, K.; Liu, F.; Long, J.; Hu, H.; Gao, H.; Wu, Q. Synthesis and characterization of a series of 2-aminopyridine nickel (II) complexes and their catalytic properties toward ethylene polymerization. *J. Polym. Sci. A Polym. Chem.* **2008**, *46*, 1618–1628. [CrossRef]
32. Sun, W.-H.; Song, S.; Li, B.; Redshaw, C.; Hao, X.; Li, Y.-S.; Wang, F. Ethylene polymerization by 2-iminopyridylnickel halide complexes: Synthesis, characterization and catalytic influence of the benzhydryl group. *Dalton Trans.* **2012**, *41*, 11999–12010. [CrossRef]
33. Jia, D.; Zhang, W.; Liu, W.; Wang, L.; Redshaw, C.; Sun, W.-H. Unsymmetrical α-diiminonickel bromide complexes: Synthesis, characterization and their catalytic behavior toward ethylene. *Catal. Sci. Technol.* **2013**, *3*, 2737–2745. [CrossRef]
34. Liu, Q.; Zhang, W.; Jia, D.; Hao, X.; Redshaw, C.; Sun, W.-H. 2-{2,6-Bis[bis(4-fluorophenyl)methyl]-4-chlorophenylimino}- 3-aryliminobutylnickel (II) bromide complexes: Synthesis, characterization, and investigation of their catalytic behavior. *Appl. Catal. A Gen.* **2014**, *475*, 195–202. [CrossRef]
35. Gao, M.; Du, S.; Ban, Q.; Xing, Q.; Sun, W.-H. Ethylene polymerization by 2,3-diiminobutylnickel bromide pre-catalysts bearing remote benzhydryl substituents. *J. Organomet. Chem.* **2015**, *798*, 401–407. [CrossRef]
36. Wang, X.; Fan, L.; Ma, Y.; Guo, C.-Y.; Solan, G.A.; Sun, Y.; Sun, W.-H. Elastomeric polyethylenes accessible via ethylene homo-polymerization using an unsymmetrical α-diimino-nickel catalyst. *Polym. Chem.* **2017**, *8*, 2785–2795. [CrossRef]
37. Wen, C.; Yuan, S.; Shi, Q.; Yue, E.; Liu, D.; Sun, W.-H. Tailoring polyethylenes by nickel complexes bearing modified 1-(2-benzhydrylnaphthylimino)-2-phenyliminoacenaphthylene derivatives. *Organometallics* **2014**, *33*, 7223–7231. [CrossRef]
38. Du, S.; Xing, Q.; Flisak, Z.; Yue, E.; Sun, Y.; Sun, W.-H. Ethylene polymerization by the thermally unique 1-[2-(bis (4-fluoro phenyl) methyl)-4, 6-dimethylphenylimino]-2-aryliminoacenaphthylnickel precursors. *Dalton Trans.* **2015**, *44*, 12282–12291. [CrossRef]
39. Du, S.; Kong, S.; Shi, Q.; Mao, J.; Guo, C.; Yi, J.; Liang, T.; Sun, W.-H. Enhancing the activity and thermal stability of nickel complex precatalysts using 1-[2, 6-bis (bis (4-fluorophenyl) methyl)-4-methyl phenylimino]-2-aryliminoacenaphthylene derivatives. *Organometallics* **2015**, *34*, 582–590. [CrossRef]

40. Fan, L.; Yue, E.; Du, S.; Guo, C.-Y.; Hao, X.; Sun, W.-H. Enhancing thermo-stability to ethylene polymerization: Synthesis, characterization and the catalytic behavior of 1-(2,4-dibenzhydryl-6-chlorophenylimino)-2-aryliminoacenaphthylnickel halides. *RSC Adv.* **2015**, *5*, 93274–93282. [CrossRef]
41. Yuan, S.; Yue, E.; Wen, C.; Sun, W.-H. Synthesis, characterization, and ethylene polymerization of 1-[2,4-bis(bis(4-fluorophenyl)methyl)naphthylimino]-2-aryliminoacenaphthylnickel bromides: Influences of polymerization parameters on polyethylenes. *RSC Adv.* **2016**, *6*, 7431–7438. [CrossRef]
42. Liu, H.; Zhao, W.; Hao, X.; Redshaw, C.; Huang, W.; Sun, W.-H. 2, 6-Dibenzhydryl-*N*-(2-phenyliminoacenaphthylenylidene)-4-methylbenzenamine nickel dibromides: Synthesis, characterization, and ethylene polymerization. *Organometallics* **2011**, *30*, 2418–2424. [CrossRef]
43. Kong, S.; Guo, C.-Y.; Yang, W.; Wang, L.; Sun, W.-H.; Glaser, R. 2, 6-Dibenzhydryl-*N*-(2-phenyliminoacenaphthylenylidene)-4-chloro-aniline nickel dihalides: Synthesis, characterization and ethylene polymerization for polyethylenes with high molecular weights. *J. Organomet. Chem.* **2013**, *725*, 37–45. [CrossRef]
44. Fan, L.; Du, S.; Guo, C.Y.; Hao, X.; Sun, W.H. 1-(2,6-dibenzhydryl-4-fluorophenylimino)-2-aryliminoacenaphthylylnickel halides highly polymerizing ethylene for the polyethylenes with high branches and molecular weights. *J. Polym. Sci. A Polym. Chem.* **2015**, *53*, 1369–1378. [CrossRef]
45. Mahmood, Q.; Zeng, Y.; Wang, X.; Sun, Y.; Sun, W.-H. Advancing polyethylene properties by incorporating NO2 moiety in 1,2-bis(arylimino)acenaphthylnickel precatalysts: Synthesis, characterization and ethylene polymerization. *Dalton Trans.* **2017**, *46*, 6934–6947. [CrossRef] [PubMed]
46. Mahmood, Q.; Zeng, Y.; Yue, E.; Solan, G.A.; Liang, T.; Sun, W.-H. Ultra-high molecular weight elastomeric polyethylene using an electronically and sterically enhanced nickel catalyst. *Polym. Chem.* **2017**, *8*, 6416–6430. [CrossRef]
47. Chen, Y.; Du, S.; Huang, C.; Solan, G.A.; Hao, X.; Sun, W.H. Balancing high thermal stability with high activity in diaryliminoacenaphthene-nickel (II) catalysts for ethylene polymerization. *J. Polym. Sci. A Polym. Chem.* **2017**, *55*, 1971–1983. [CrossRef]
48. Britovsek, G.J.; Cohen, S.A.; Gibson, V.C.; Van Meurs, M. Iron catalyzed polyethylene chain growth on zinc: A study of the factors delineating chain transfer versus catalyzed chain growth in zinc and related metal alkyl systems. *J. Am. Chem. Soc.* **2004**, *126*, 10701–10712. [CrossRef]
49. Wang, X.; Fan, L.; Yuan, Y.; Du, S.; Sun, Y.; Solan, G.A.; Guo, C.-Y.; Sun, W.-H. Raising the N-aryl fluoride content in unsymmetrical diaryliminoacenaphthylenes as a route to highly active nickel (II) catalysts in ethylene polymerization. *Dalton Trans.* **2016**, *45*, 18313–18323. [CrossRef]
50. Mahmood, Q.; Li, X.; Qin, L.; Wang, L.; Sun, W.H. Structural evolution of pyridinylimine support for nickel/palladium catalysts in ethene (oligo)polymerization. *Dalton Trans.* **2022**, *51*, 14375–14407. [CrossRef]
51. Huang, F.; Sun, Z.; Du, S.; Yue, E.; Ba, J.; Hu, X.; Liang, T.; Galland, G.B.; Sun, W.-H. Ring-tension adjusted ethylene polymerization by aryliminocycloheptapyridyl nickel complexes. *Dalton Trans.* **2015**, *44*, 14281–14292. [CrossRef]
52. Sun, Z.; Huang, F.; Qu, M.; Yue, E.; Oleynik, I.V.; Oleynik, I.I.; Zeng, Y.; Liang, T.; Li, K.; Zhang, W. Targeting polyethylene waxes: 9-(2-cycloalkylphenylimino)-5,6,7,8-tetrahydrocycloheptapyridylnickel halides and their use as catalysts for ethylene polymerization. *RSC Adv.* **2015**, *5*, 77913–77921. [CrossRef]
53. Zhang, T.; Guo, D.; Jie, S.; Sun, W.H.; Li, T.; Yang, X. Influence of electronic effect on catalytic activity of salicylaldiminato nickel (II) complexes. *J. Polym. Sci. A Polym. Chem.* **2004**, *42*, 4765–4774. [CrossRef]
54. Yang, W.; Yi, J.; Sun, W.H. Revisiting benzylidenequinolinylnickel catalysts through the electronic effects on catalytic activity by DFT studies. *Macromol. Chem. Phys.* **2015**, *216*, 1125–1133. [CrossRef]
55. Liu, H.; Zhao, W.; Yu, J.; Yang, W.; Hao, X.; Redshaw, C.; Chen, L.; Sun, W.-H. Synthesis, characterization and ethylene polymerization behavior of nickel dihalide complexes bearing bulky unsymmetrical α-diimine ligands. *Catal. Sci. Technol.* **2012**, *2*, 415–422. [CrossRef]
56. Galland, G.B.; de Souza, R.F.; Mauler, R.S.; Nunes, F.F. 13C NMR determination of the composition of linear low-density polyethylene obtained with [η3-methallyl-nickel-diimine] PF6 complex. *Macromolecules* **1999**, *32*, 1620–1625. [CrossRef]
57. Galland, G.B.; Quijada, R.; Rojas, R.; Bazan, G.; Komon, Z.J. NMR study of branched polyethylenes obtained with combined Fe and Zr catalysts. *Macromolecules* **2002**, *35*, 339–345. [CrossRef]
58. Busico, V.; Cipullo, R.; Friederichs, N.; Linssen, H.; Segre, A.; Van Axel Castelli, V.; van der Velden, G. H NMR analysis of chain unsaturations in ethene/1-octene copolymers prepared with metallocene catalysts at high temperature. *Macromolecules* **2005**, *38*, 6988–6996. [CrossRef]
59. Popeney, C.S.; Rheingold, A.L.; Guan, Z. Nickel (II) and palladium (II) polymerization catalysts bearing a fluorinated cyclophane ligand: Stabilization of the reactive intermediate. *Organometallics* **2009**, *28*, 4452–4463. [CrossRef]
60. Ahmadjo, S.; Damavandi, S.; Zohuri, G.; Farhadipour, A.; Etemadinia, Z. Mechanisms for the effects of fluorine and α-diimine backbone structure on the catalyst behavior and catalyst deactivation in ethylene polymerization by Ni catalysts. *J. Organomet. Chem.* **2017**, *835*, 43–51. [CrossRef]
61. Guo, L.; Zhu, D.; Zhang, W.; Zada, M.; Solan, G.A.; Hao, X.; Sun, W.-H. Remote dibenzocycloheptyl-substitution of an iminotrihydroquinoline-nickel catalyst as a route to narrowly dispersed branched polyethylene waxes with alkene functionality. *Eur. Polym. J.* **2018**, *107*, 315–328. [CrossRef]

62. Zada, M.; Guo, L.; Zhang, R.; Zhang, W.; Ma, Y.; Solan, G.A.; Sun, Y.; Sun, W.H. Moderately branched ultra-high molecular weight polyethylene by using N,N′-nickel catalysts adorned with sterically hindered dibenzocycloheptyl groups. *Appl. Organomet. Chem.* **2019**, *33*, e4749. [CrossRef]
63. Meiries, S.; Speck, K.; Cordes, D.B.; Slawin, A.M.; Nolan, S.P. [Pd (IPr* OMe)(acac) Cl]: Tuning the N-heterocyclic Carbene in catalytic C–N bond formation. *Organometallics* **2013**, *32*, 330–339. [CrossRef]
64. Rosa, V.; Avilés, T.; Aullon, G.; Covelo, B.; Lodeiro, C. A new bis (1-naphthylimino) acenaphthene compound and its Pd (II) and Zn (II) complexes: Synthesis, characterization, solid-state structures and density functional theory studies on the syn and anti isomers. *Inorg. Chem.* **2008**, *47*, 7734–7744. [CrossRef]
65. Vasudevan, K.V.; Findlater, M.; Cowley, A.H. Synthesis and reactivity of tetrakis (imino)pyracene (TIP) ligands; bifunctional analogues of the BIAN ligand class. *Chem. Commun.* **2008**, *16*, 1918–1919. [CrossRef]
66. Dolomanov, O.V.; Bourhis, L.J.; Gildea, R.J.; Howard, J.A.K.; Puschamann, H. OLEX2 A Complete Structure Solution, Refinement and Analysis Program. *J. App. Cryst.* **2009**, *42*, 339–341. [CrossRef]
67. Sheldrick, G.M. Crystal structure refinement with SHELXL. *Acta Crystallogr. C Struct. Chem.* **2015**, *71*, 3–8. [CrossRef]
68. Sheldrick, G.M. SHELTX-integrated space-group and crystalstructure determination. *Acta Crystallogr. Sect. A Found. Adv.* **2015**, *71*, 3–8. [CrossRef]